Continental Shelf Research 295 (2025) 105565

Contents lists available at ScienceDirect

Continental Shelf Research

journal homepage: www.elsevier.com/locate/csr

Analysis of the uncertainties in tidal constants obtained from short tide gauge records and their value for tidal studies

M.S. Filmer [a,*], P.L. Woodworth [b], S.D.P. Williams [b], S.J. Claessens [a]

[a] School of Earth and Planetary Sciences, Curtin University, GPO Box U1987, Perth, WA 6845, Australia
[b] National Oceanography Centre, Joseph Proudman Building, 6 Brownlow Street, Liverpool, L3 5DA, UK

ARTICLE INFO

Keywords:
Ocean tides
Tide gauge records
Tidal inference
Tidal constituent uncertainties
Ocean tide models

ABSTRACT

We conduct a study to estimate uncertainties in tidal constants from M2, S2, N2, K1, O1, Q1 and related K2, P1, 2N2 constituents from 35-day tide gauge records in the northern Australia and Papua New Guinea regions. The motivation for this study stems from the availability of ~300 short tide gauge records (most ~ 30 days long) in these regions, but their accuracy for tidal studies is not clear. We simulate the 35-day uncertainties by dividing a selected set of 14 long tide gauge records (19-years where available) from the GESLA3 data set into consecutive 35-day sections. Amplitudes and phase lags computed from each long record are treated as the 'true' values, from which we compute and analyse inference information for the short records. Comparison of empirical amplitude ratios and phase lag differences with the relationships from the Equilibrium tide show significant differences in both amplitude and phase lag in some constituents and locations. We also compare inference information derived from the FES2022b ocean tide model, which suggests that such models could be used in this way in some instances. Empirical uncertainties in the 35-day records were no more than 0.045 m with maximum errors reaching 0.093 m. The largest 35-day errors appeared in the K1 constituent, mostly in the Torres Strait and northwest Australia. Empirical inference information showed improvement on the Equilibrium assumption for S2 and K1 reference constituents and related constituents K2, 2N2 and P1, demonstrating that the latter can be accurately derived from short records with accurate inference information.

1. Introduction

A knowledge of ocean tides at the coast is required for a range of applications, e.g., navigation and coastal management, including studies of inundation from storm surges and rising sea levels. Tidal information can be obtained in coastal regions from the sea level records of permanent tide gauge installations in ports and harbours. Temporary tide gauge installations used in coastal surveying and scientific research can also provide useful information (Woodworth et al., 2015). In addition, tidal information can be extracted from ocean tide models; either 'pure' hydrodynamic models or ones derived from assimilation of satellite altimeter data. The tide-producing potential is conventionally parameterised as a set of harmonics with specific frequencies that depend upon the relative positions of the Earth, Sun and Moon. These various harmonics separate into 'species', 'groups' and 'constituents' (Cartwright and Tayler, 1971; Pugh and Woodworth, 2014). The tide observed at a particular location in the real ocean is then considered as the ocean's frequency-dependent response to the potential. That response is usually expressed in terms of a set of 'tidal constants', referring to the amplitudes and phase lags of particular harmonics at a specific location. We will use the term 'constituent' or 'constant' on this basis somewhat interchangeably throughout this paper.

Permanent tide gauge installations provide the long tide gauge records that sometimes extend over decades, with any gaps in the records due to occasional tide gauge malfunction or damage. These data are our best information of tides, but they are sparsely distributed along the coast. Ocean tide models (OTMs, e.g., Lyard et al., 2021; Egbert and Erofeeva, 2002; Hart-Davis et al., 2021) offer higher spatial resolution: for example, FES2022b (Carrère et al., 2022; Lyard et al., in prep.) tides are available on a 1/30° by 1/30° grid, and can supply tidal constants for coastal locations but, despite recent improvements, these are less reliable close to the coast (e.g., Birol et al., 2017; Seifi and Filmer, 2023). This is exacerbated in regions with partially enclosed bays, irregularly shaped coastlines and shallow bathymetry (Ray et al., 2011; Egbert et al., 2010). New results from the SWOT satellite mission may significantly improve these results in coastal regions in the near future

* Corresponding author.
E-mail address: M.Filmer@curtin.edu.au (M.S. Filmer).

https://doi.org/10.1016/j.csr.2025.105565
Received 24 April 2025; Received in revised form 29 August 2025; Accepted 1 September 2025
Available online 2 September 2025

(Morrow et al., 2019; Hart-Davis et al., 2024).

Temporary tide gauges are installed in many instances to obtain tides for specific reasons, often from only one month of observations. Examples of these could be local surveying projects that need tidal levels for chart datum determination, for extending nautical charts, or for maritime navigation, or sometimes for naval defence purposes. The drawback with temporary tide gauge installations is that due to their short records, it is only possible to resolve a small number of tidal constituents, often with uncertainty as to the accuracy of their amplitudes and phase lags obtained from the harmonic analysis (cf. Pawlowicz et al., 2002). These uncertainties are likely to vary spatially due to the variation of tidal characteristics in different coastal locations and in time, depending on the time of year when the one-month record is observed. On the other hand, an advantage of short tide gauge records is that, in principle, there will generally be many more such installations across a region and will therefore provide a much better coverage of the tides in these particular areas than the sparse permanent coastal tide gauge network.

We have one such data set of 312 short tide gauge records (with length of around one month; see below) available to us from the Australian Hydrographic Office (AHO) which extends across northern Australian and the Papua New Guinea (PNG) region. These short tide gauge records are a considerable increase on the limited number used in the studies of Seifi and Filmer (2023) and Filmer et al. (2024) in north west Australia. Therefore, the motivation for the present study is to estimate the uncertainty of the amplitudes and phase lags that can be reliably extracted from harmonic analysis of short (one month) tide gauge records. For this study, we do not actually use these 312 short records themselves, but instead we use long tide gauge records in these regions to estimate how accurately any tidal constants derived from the short records can be estimated. The 312 short tide gauges are being used in a scientific study (with manuscript in preparation) which will be underpinned by the uncertainty analysis in this article.

The long tide gauge records are divided into 35-day segments from which short record constants can be estimated and analysed using the long record constants as the 'true values'. The AHO short tide gauge records available to us are mostly around 30-days in length, but current AHO requirements for the Hydrosphere Industry Partnership Program (HIPP, see https://www.hydro.gov.au/NHP/hipp.htm and AHO, 2024) specify that short tide gauge installations should provide 35-days of continuous observation. Following this, we adopt 35-days as standard length for 'short' tide gauges in this study. Knowledge of the accuracies of the short record constants will enable a clearer understanding of the overall value of the short records for a range of tidal studies, which is the objective of this study.

Short tide gauge records of 35 days will allow a number of constituents to be resolved. The Rayleigh criterion is often used as a guide to decide which constituents should be included in a harmonic analysis. This specifies the length of time required to separate neighbouring constituents and is computed as $360/\Delta s$ where Δs is the difference in speed (in degrees per hour) between the two neighbouring constituents. Pugh and Woodworth (2014), for example (see also Parker, 2007; Table A1), show that to separate M2 from S2 requires 360/(30.0000000–28.9841042) hours = 14.77 days which is a complete spring-neap cycle. On the other hand, to separate K2 from S2 requires 360/(30.0821373–30.000000) hours = 182.6 days. The minimum record length needed to separate a pair of constituents is called their synodic period. Hence, in theory, 35-day tide gauge records cannot separate the K2 constituent from S2, nor P1 from K1 which requires 360/(15.0410686–14.9589314) = 182.6 days.

In this instance, a long tide gauge record of a reference (permanent installation) tide gauge can be used to estimate the empirical amplitude ratio and phase lag difference between two constituents with similar periods. For example, the ratio of the amplitude of K2 to that of S2 and the phase lag difference between K2 and S2 can be determined from the long record. These relationships can then be assumed in the harmonic analysis of any nearby short record. Thereby, the amplitude and phase lag of the smaller 'related' constituent is defined in relation to those of the larger 'reference' constituent through the method of inference. Previous studies on the harmonic analysis of short tide gauge records and methods of inference include Parker (2007), who discusses the earlier work of Schureman (1958) and Godin (1972). Foreman (2004) developed a method based on that of Godin (1972) to interrelated constituents that otherwise could not be separated from their reference constituents in the short tide gauge records. Ray (2017) developed a refined methodology for inference in the diurnal tidal band (K1 tidal group), focussing on the effect of the 'nearly diurnal free wobble' (NDFW). The NDFW was shown to have a real, but negligible effect on the estimated constituents from one-month of tide gauge data. A notable finding from Ray (2017) was empirical evidence that the amplitude ratio for P1/K1 is closer to 0.318 than the value of 0.331 shown in Godin (1972) and also in Pugh and Woodworth (2014).

When there is no long reference tide gauge record available near the location of the temporary tide gauge installation, then Equation (4.7) in Pugh and Woodworth (2014) shows the relationships between related and reference constituents in the Equilibrium Tide that might be used instead of the empirically estimated values

$$\alpha_E = \frac{\text{related constituent amplitude}}{\text{reference constituent amplitude}} \tag{1}$$

$$\beta_E = \text{related constituent phase - reference constituent phase} \tag{2}$$

Equilibrium relationship values for α_E and β_E can be found in Table 4.5 of Pugh and Woodworth (2014). In theory, the Equilibrium relationships are global constants, but shallow waters, especially at coastal barriers will lead to variation in these values that should then be estimated from local tides. Eq. (1) and Eq. (2) can be used in this way to estimate empirical amplitude ratios and phase lag differences, noting that the subtraction order in Eq. (2) may vary depending on the harmonic analysis software used to compute the constituents.

There are then two approaches to inference for short tide gauge records. One is to use the Equilibrium relationship values (see Section 2) on the assumption that they vary by only small amounts in different regions, while the other is to estimate empirical amplitude ratio and phase lag difference from the long tide gauge record for specific locations. We propose an extension to this where an ocean tide model (OTM) may also be used to obtain the amplitude ratio and phase lag difference, by using the modelled tidal values in Eq. (1) and Eq. (2). All methods will have associated uncertainties: the Equilibrium relationships will vary from their values in some regions, notably in shallow coastal waters with complex coastlines; on the other hand, the empirical values are usually estimated from long tide gauges located in shallow coastal regions, so will also inevitably vary from these values in different coastal regions. Values from the modelled tides will vary in coastal regions, perhaps by large amounts in challenging regions at the coast.

2. Analysis and data

We first determine which constituents will be used in the study. Our intention is to estimate uncertainties for as many constituents as possible, but this is limited by the significance of the uncertainty with respect to its amplitude. For example, small amplitude tides that are only ~0.01 m may have uncertainties larger than their amplitude, so do not add anything significant to the study. Following our initial uncertainty analysis (see Section 3.2) we selected nine constituents that were considered significant from the 35-day record. These are the reference constituents M2, S2, N2 (semi-diurnal), K1, O1, Q1 (diurnal) and the related constituents (K2, 2N2, P1) that can not be resolved in a 35-day record according to the Rayleigh criterion but can be computed via inference.

We then selected 14 long tide gauge records from the GESLA3 database (Haigh et al., 2022; Woodworth et al., 2017; Caldwell et al.,

2015) data from https://gesla787883612.wordpress.com/downloads/), that were available within the area covered by the 312 short tide gauges (Fig. 1) and identified the longest sections of useable data. These long sections of the observed record were ideally 19 years long (to remove the 18.6 year nodal tide), but some were shorter. This was necessitated by gaps in the long tide gauge record that make some segments of the long record unusable. These 14 GESLA tide gauge records serve as the 'long records' used for comparison with the individual 35-day sections. For each long record, a full set of 62 constituents (including 5 long period tides; this full list of 62 constituents is available in the supplement of Woodworth and Vassie, 2022) was computed using the UTide software (Codiga, 2011). The constituents used were those suggested as suitable by the National Oceanography Centre (NOC) for analysis of tide gauge records of more than 1 year (minus MP1, M1, MNS2 and KJ2 which are not available in UTide).

The UTide computations to estimate tidal constants from the 19-year records used white noise estimation and ordinary least squares (OLS) options because using the more sophisticated ILRS (iteratively re-weighted least squares) with coloured noise estimation method (Codiga, 2011) was computationally excessive. Eq. (1) and Eq. (2), were used to compute the empirical amplitude ratios and phase lag differences of the eight related constituents (Pugh and Woodworth, 2014) for each long record. Eq. (2) was adapted to reference phase lag minus related phase lag because this is the order subsequently required for UTide. Equilibrium nodal variations for each constituent were applied through the UTide nodal correction.

Table 1 shows the related and reference constituents used, together with the relationships in the Equilibrium Tide which are taken from Pugh and Woodworth (2014). The P1/K1 ratio of 0.331 in the Equilibrium Tide in Table 1 is as given in Pugh and Woodworth (2014) and other tidal text books; we have used this value for consistency with previous publications, noting the value of 0.318 in Ray et al. (2011) due to a free rotational mode of the Earth in the diurnal band. To test the validity of the different inference methods (Equilibrium relationships and empirical values) we will apply each in two different UTide estimations of 35-day amplitudes and phase lags. We will focus on direct comparisons of amplitude ratios and phase lag differences for four related constituents with the largest ratios P1/K1, 2N2/N2, NU2/N2, K2/S2. These will have large enough tidal amplitudes to be important in the uncertainty analysis and indicate significant differences among the Equilibrium relationships and the empirical values. We also test the validity of amplitude ratios and phase lag differences extracted from OTM tides for inference of short tide gauge records. The OTM values are computed from Eq. (1) and Eq. (2) using modelled tides from FES2022b (https://www.aviso.altimetry.fr/en/data/products/auxiliary-products/global-tide-fes.html) at the nearest grid point to the position of each of the 14 long tide gauges.

Table 1
Related and reference constituents used in the computation of tidal constants from 35-day tide gauge records (from Table 4.5 in Pugh and Woodworth, 2014). Synodic period was either taken from Table 39 of Schureman (1958) or where marked with (*) the value was calculated using the Rayleigh criterion using values from Table A1 in Parker (2007).

Related constituent	Reference constituent	Equilibrium relationships α_E	Equilibrium relationships β_E	Synodic period (days)
PI1	K1	0.019	0.0	121.8*
P1	K1	0.331	0.0	182.6
PSI1	K1	0.008	0.0	365.3*
PHI1	K1	0.014	0.0	182.6*
2N2	N2	0.133	0.0	27.6*
NU2	N2	0.194	0.0	205.9
T2	S2	0.059	0.0	365.3
K2	S2	0.272	0.0	182.6

Each 19-year record was divided into 35-day segments to create a time series of 35-day tide gauge records. We use 35-days (solar days) as per the AHO (2024) requirement for short tide gauge observations, but also as it exceeds a lunar month by a few days which allows us to apply a condition that requires at least 95 % of the full 35-day record to be used in the analysis. If the 35-day segment has less than 95 % data, it is

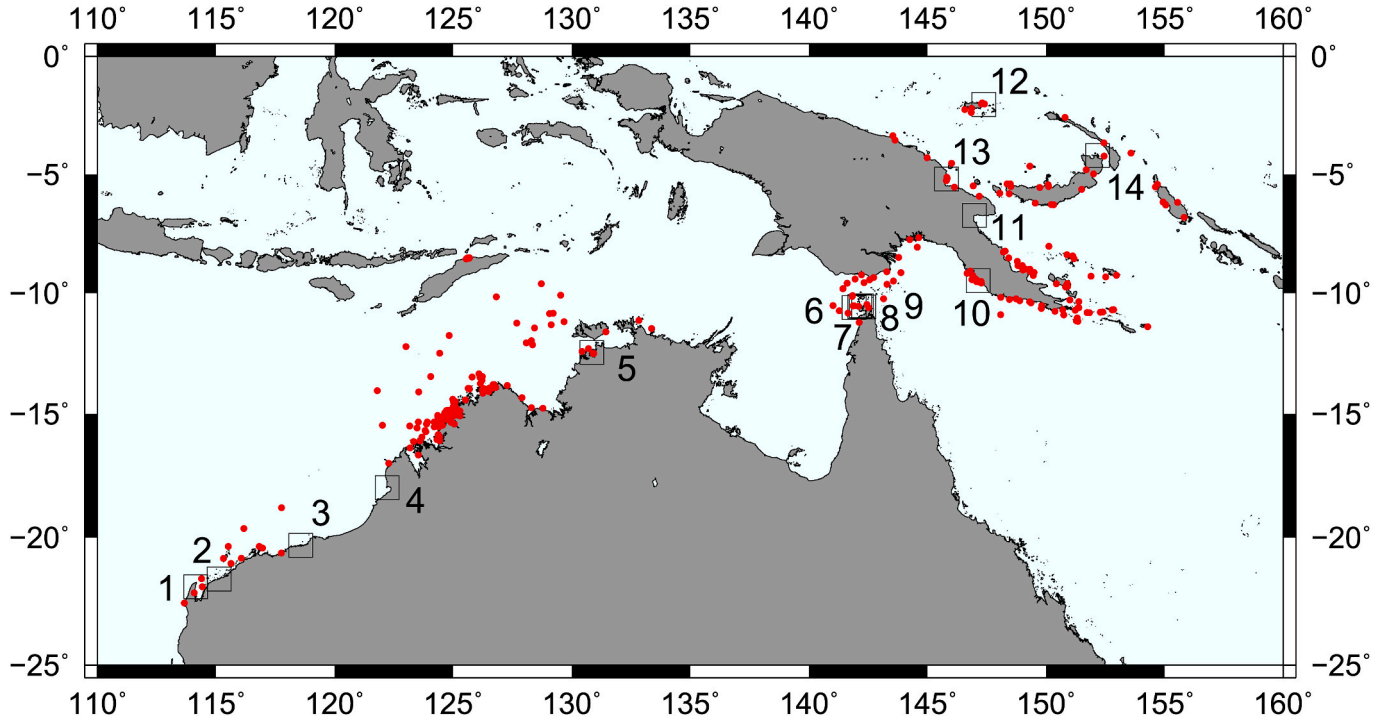

Fig. 1. Locations of AHO short term tide gauges (red circles), and those of the GESLA3 long tide gauge records shown as black hollow squares, to demonstrate the regions where a long-term tide gauge record can be used to estimate uncertainty in the short records. The GESLA tide gauges are numbered as per Table 2. (For interpretation of the references to colour in this figure legend, the reader is referred to the Web version of this article.)

Table 2
GESLA3 tide gauges with the time span and record length in years used for this study. Records of 19 years were used where possible. Shorter records had to be used where there were large gaps in the tide gauge record.

Tide gauge site	Region	TG#	Time span of record	Record length (yrs)	Longitude (deg E)	Latitude (deg S)
Exmouth	W	1	01/01/1998-01/01/2016	18	114.1409	21.9549
Onslow Beadon Creek	W	2	01/01/2000-01/01/2019	19	115.1315	21.6497
Port Hedland	W	3	01/01/1992-01/01/2011	19	118.575	20.318
Broome	NW	4	01/01/2000-01/01/2019	19	122.2186	18.0008
Darwin	NW	5	01/01/2000-01/01/2019	19	130.8459	12.4718
Booby Island	TS	6	01/01/2000-01/01/2019	19	141.9101	10.6026
Goods Island	TS	7	30/04/1998-21/02/2013	14.7	142.1486	10.5639
Turtle Head	TS	8	01/01/2000-01/01/2019	19	142.2133	10.5212
Ince Point	TS	9	01/01/2001-01/01/2010	9	142.3117	10.5750
Port Moresby	SE PNG	10	01/01/1985-01/01/1992	7	147.1400	9.4780
Lae	N PNG	11	01/01/1991-25/06/1994	3.5	146.9830	6.7330
Lombrum-Manus	N PNG	12	01/01/2000-01/01/2014	14	147.3750	2.0370
Madang	N PNG	13	25/08/1984-25/09/1991	7	145.8000	5.2000
Rabaul	N PNG	14	01/01/1975-01/01/1994	19	152.1750	4.2000

removed from the analysis to avoid biasing the results. Amplitudes and phase lags were computed for all 35-day sections using 25 reference and eight related constituents (Bell et al., 1996), less those for M1 which is not available in the UTide software. The amplitudes and phase lags extracted from the 35-day sections are then analysed as a time series of 35-day constituents with respect to the same constituents computed over the complete 19-years. For the purpose of this study, we consider the 19-year values to be the 'true' ones, while acknowledging that they will inevitably contain their own (small) uncertainties, and that some of the long tide gauge records are shorter than 19 years (as shown in Table 2).

We will compute statistics of these time series of 35-day segments, with the RMS computed as

$$RMS = \sqrt{\frac{1}{N}\sum_{n=1}^{N}|x_n|^2} \tag{3}$$

where x is the difference between the 35-day constituent values and the long record values, with ($n = 1,2,3\ldots N$) and N is the number of 35-day segments for the long record. RMS is used as a proxy for the uncertainty, with the maximum and minimum difference of the 35-day record to the long record indicating the largest possible error in a 35-day tide gauge record, and the mean difference is an indication of any bias in the 35-day record. The RMS is chosen rather than standard deviation as it will accommodate any deviation in the mean that will impact the uncertainties. The analysis will further evaluate these findings with respect to their region and time of year, so as to identify any other error characteristics that may appear in the 35-day analyses.

Fig. 1 shows the locations of the 312 short tide gauge records (mostly 30–60 days long) in our study area. As stated in Section 1, we do not use data from these records in the present study. Rather, we are attempting to learn whether tidal information obtained from them will have future utility, by focussing on assessing the uncertainties in tidal constants in the 35-day sections of the 14 longer records in the same area. These 14 long tide gauge records from GESLA3 are listed in Table 2 and shown in Fig. 1. Subset regions of interest are delineated as shown in Fig. 1, grouped as per the numbers in Table 2: west Australia (W, tide gauges 1–3); northwest Australia (NW, tide gauges 4–5); Torres Strait (TS, tide gauges 6–9); south east PNG (SE PNG, tide gauge 10); north PNG (N PNG, tide gauges 11–14). Each of these regions tend to have distinct tidal characteristics and should be considered separately to gain a deeper insight into the tides and the ratios in these specific regions.

3. Results and discussion

3.1. Inference comparison

First, we show amplitude ratios and phase lag differences in Tables 3 and 4 respectively, computed from the 14 long records. Amplitudes and phase lags from the 14 long tide gauges are shown in Appendix 1 (Table A.1) and Appendix 2 (Table A.2) respectively. The four largest amplitude ratios P1/K1, 2N2/N2, NU2/N2, K2/S2 and their phase lag differences are shown in Fig. 2. This compares the empirical values from the 14 long tide gauge records, the Equilibrium relationships which are constant values (zero for the phase lags) and modelled tides from FES2022b. To show spatial differences, tide gauges in the Torres Strait (Fig. 3) and Papua New Guinea (Fig. 4) are plotted with their empirical amplitude ratios, and with the corresponding amplitude ratios from FES2022b for comparison. This provides an indication of where ratios computed from OTMs could possibly also be used to infer related constituents for short term tide gauges.

The results in Table 3 indicate broad agreement between empirical amplitude ratios and the Equilibrium relationships. There are a couple of notable differences (1) the K2/S2 ratio is 0.340 at Booby Island, and (2) the P1/K1 empirical ratios are less than the Equilibrium relationship for P1/K1 of 0.331, and also the 0.318 from Ray (2017), noting that the latter study used bottom pressure gauges in the open ocean and our study is restricted to tide gauges in shallow water coastal regions. The empirical phase lag differences are in Table 4 and are somewhat more complex to analyse. All Equilibrium phase lag differences are zero. It appears that the largest empirical differences (some reaching almost 180°) appear with the smallest empirical amplitude ratios. Tables 3 and 4 results are better demonstrated in Fig. 2, with a comparison to the FES2022b values and the Equilibrium relationships.

Fig. 2 demonstrates the generally good agreement between the FES2022b amplitude ratios and phase lag differences and the empirical ones from the 14 tide gauges. The FES2022b tides (on a 1/30° by 1/30° grid) are extracted from the nearest grid point to the long tide gauge coordinates. This means that no FES2022b grid point values should be more than 1 arc minute (~1.8 km) from a tide gauge. The empirical amplitude ratios from the 14 tide gauge are considered to be the 'truth' with negligible uncertainty for this comparison, so that the differences shown here are assumed to be FES2022b modelling error. Uncertainty estimates are unavailable for FES2022b, but Lyard et al. (2021) suggest vector differences to coastal tide gauges for FES2014 of ~3.5 cm (S2) and ~3 cm (K1), with N2 differences unavailable. If we use these as a (crude) 'proxy' uncertainty for the P1/K1 and K2/S2 FES2022b amplitude ratios, it appears that most comparisons are within uncertainty, with K2/S2 amplitude ratio in the diurnal north PNG region appearing the outliers. Other key points from Fig. 2 are the P1/K1 amplitude ratios all below the Equilibrium relationship (0.331) and also mostly below 0.318 from Ray (2017). The amplitude ratio through the Torres Strait for some constituent pairs is captured accurately by FES2022b in most instances, but NU2/N2 shows some large differences for the western end of Torres Strait. The phase lag step for K2/S2 through the Torres Strait is

Table 3
Empirical amplitude ratios computed from the 14 GESLA long tide gauge records. The Equilibrium relationships are shown for reference on the top row. The different spatial regions are alternately shaded grey and white.

Tide gauge site	Tide gauge #	PI1/K1	P1/K1	PSI1/K1	PHI1/K1	2N2/N2	NU2/N2	T2/S2	K2/S2
Equilibrium relationships		**0.019**	**0.331**	**0.008**	**0.014**	**0.133**	**0.194**	**0.059**	**0.272**
Exmouth (W)	1	0.016	0.308	0.006	0.009	0.109	0.186	0.048	0.278
Onslow Beadon Creek (W)	2	0.017	0.305	0.010	0.009	0.110	0.190	0.055	0.276
Port Hedland (W)	3	0.019	0.286	0.008	0.013	0.103	0.197	0.051	0.283
Broome (NW)	4	0.028	0.277	0.019	0.013	0.101	0.194	0.050	0.282
Darwin (NW)	5	0.025	0.276	0.019	0.018	0.116	0.190	0.055	0.280
Booby Island (TS)	6	0.022	0.258	0.019	0.019	0.146	0.217	0.052	0.340
Goods Island (TS)	7	0.021	0.255	0.021	0.017	0.157	0.223	0.047	0.259
Turtle Head (TS)	8	0.025	0.268	0.020	0.019	0.181	0.184	0.073	0.266
Ince Point (TS)	9	0.024	0.265	0.036	0.012	0.158	0.149	0.058	0.261
Port Moresby (SE PNG)	10	0.019	0.295	0.011	0.008	0.139	0.176	0.074	0.270
Lae (N PNG)	11	0.021	0.301	0.016	0.017	0.165	0.195	0.098	0.271
Lombrum Manus Is (N PNG)	12	0.017	0.314	0.002	0.019	0.159	0.207	0.090	0.293
Madang (N PNG)	13	0.018	0.311	0.001	0.018	0.151	0.202	0.082	0.271
Rabaul (N PNG)	14	0.017	0.296	0.008	0.014	0.171	0.220	0.092	0.291

Table 4
Empirical phase lag differences computed from the 14 GESLA long tide gauge records as per Eq. (2). The Equilibrium phase lag differences are all zero. The different spatial regions are alternately shaded grey and white.

Tide gauge site	Tide gauge #	PI1/K1	P1/K1	PSI1/K1	PHI1/K1	2N2/N2	NU2/N2	T2/S2	K2/S2
Exmouth (W)	1	-12.404	2.762	-112.273	-12.408	34.459	3.322	-14.988	2.470
Onslow Beadon Creek (W)	2	-19.108	3.973	-151.176	-18.059	34.227	-2.555	-8.203	2.141
Port Hedland (W)	3	10.698	1.236	23.724	-17.218	33.693	0.053	-5.485	1.786
Broome (NW)	4	6.483	-2.178	41.395	1.748	34.128	2.153	-2.602	2.089
Darwin (NW)	5	-3.603	-3.784	-0.190	-7.769	24.688	-5.402	-1.694	2.171
Booby Island (TS)	6	8.019	7.734	-2.713	-30.876	34.677	-6.516	37.665	27.454
Goods Island (TS)	7	7.051	8.585	-7.329	-37.049	28.928	-11.808	35.541	25.567
Turtle Head (TS)	8	8.828	7.382	-31.274	-30.386	16.438	-23.029	4.246	17.778
Ince Point (TS)	9	9.455	4.346	-19.021	-27.605	7.679	-10.843	23.673	9.888
Port Moresby (SE PNG)	10	6.705	4.241	3.219	-19.488	7.675	-4.622	18.565	3.219
Lae (N PNG)	11	-17.645	4.297	56.650	27.733	37.259	-3.650	-1.608	8.152
Lombrum Manus Island (N PNG)	12	8.811	-0.233	82.688	5.989	36.329	-10.352	-11.683	14.947
Madang (N PNG)	13	0.622	1.732	-45.244	-11.422	36.394	-3.738	-11.464	10.334
Rabaul (N PNG)	14	3.861	3.086	83.700	-3.119	42.610	-11.963	-19.045	8.777

highlighted for the tide gauges and accurately represented by FES2022b, but there is a large discrepancy for the NU2/N2 phase lag through this same region between model and tide gauge values. A key conclusion is that there is significant variation from the Equilibrium relationships with the phase lag difference to zero also prominent, which is likely to introduce errors into the 35-day constants if the Equilibrium relationships are used for inference in this region (see Section 3.2). It should also be noted that FES2022b may assimilate some tide gauges in the Torres Strait which would help explain the generally good agreement.

Fig. 3 highlights the spatial variability of the amplitude ratios in Table 3, Table 4 and Fig. 2 in the Torres Strait. All FES2022b ratios show a boundary with a steep gradient increase from west to east for P1/K1, NU2/N2 and 2N2/N2, but with a steep decrease from west to east for K2/S2. The four tide gauges we have in the Torres Strait are located on the southern (Australian) side, so we cannot confirm the FES2022b ratios on the northern side of the Torres Strait. Fig. 4 shows the same comparisons around PNG. Key points are the discrepancy for K2/S2 at Lombrum-Manus Island (12, tide gauge ratio 0.293) and Madang (13, tide gauge ratio 0.271), where the modelled negative gradient tends to zero (towards the west). This is most likely an error in the model, as it is unlikely the ratio will tend to zero. This region north of PNG has a diurnal tidal regime with very small diurnal amplitudes (see Appendix 1), with Lombrum-Manus Island tide gauge showing S2 amplitude of 0.047 m and K2 of 0.014 m, and for Madang S2 is 0.060 m and K2 0.016 m. It is possible that, if the model contains errors in this region for S2, the K2/S2 ratio may be significantly influenced. For NU2/N2, Rabaul (14), and to a lesser extent Lae (11), indicate differences. As discussed above for the K2/S2 ratio in this region, Lae, for example, has a NU2 amplitude of 0.004 m and N2 of 0.020 m, so that model errors may disproportionately influence the ratio. We do not show the spatial OTM comparisons for the west and north west areas as these indicate generally good agreement (cf. Fig. 2) so do not justify taking additional space in this paper.

The comparisons of the empirical amplitude ratios with the Equilibrium relationships suggest that at many locations it is reasonable to use the latter to infer the eight related constituents shown in Tables 3

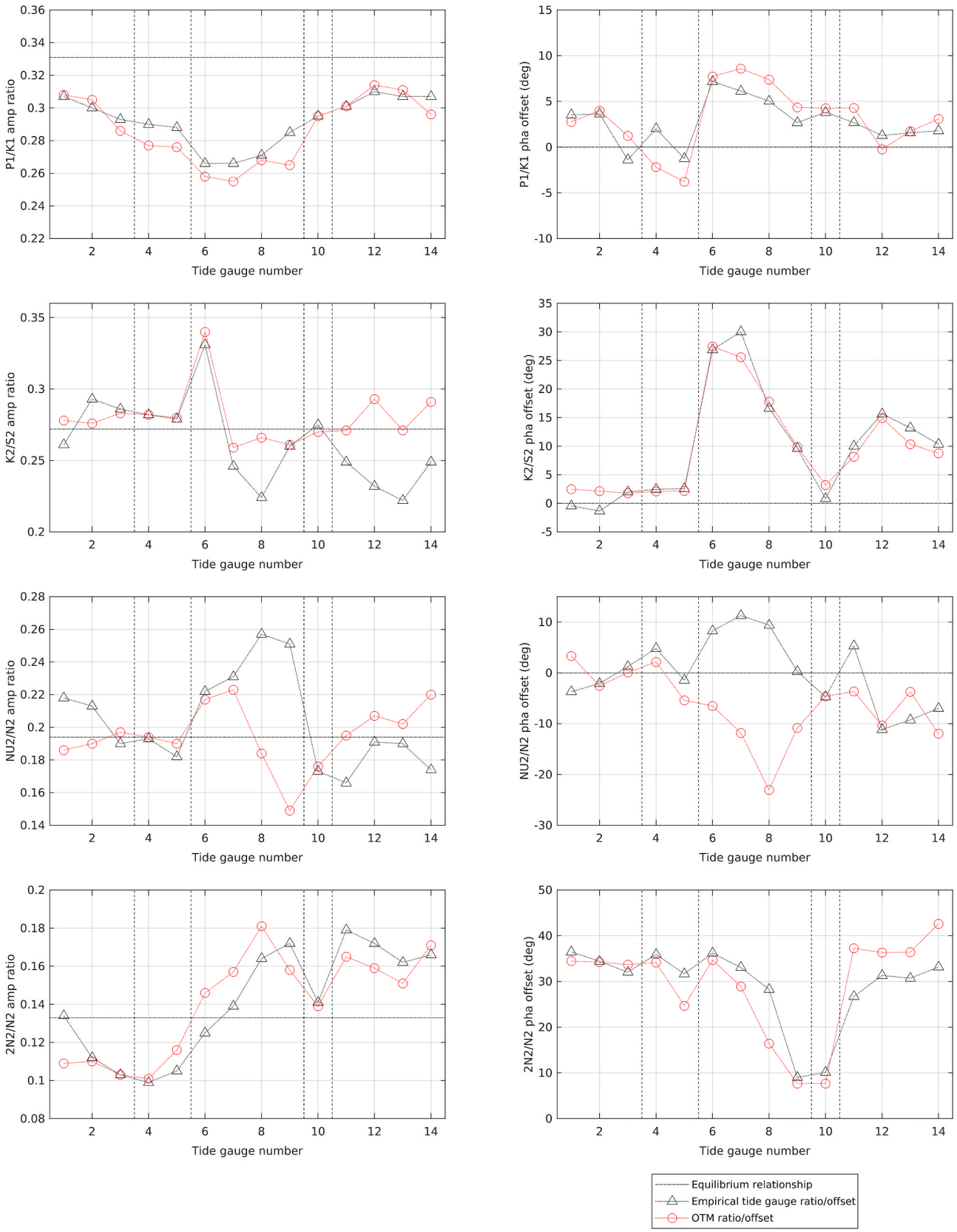

Fig. 2. Empirical amplitude ratios (left column) and phase lag differences (right column) computed from 14 GESLA3 long tide gauge records (red circles), and those from FES2022b at the tide gauge position (black triangles). Vertical dashed lines separate the different regions and the horizontal dashed and dotted line is the Equilibrium relationship value (constant in each amplitude plot and zero for each phase offset). (For interpretation of the references to colour in this figure legend, the reader is referred to the Web version of this article.)

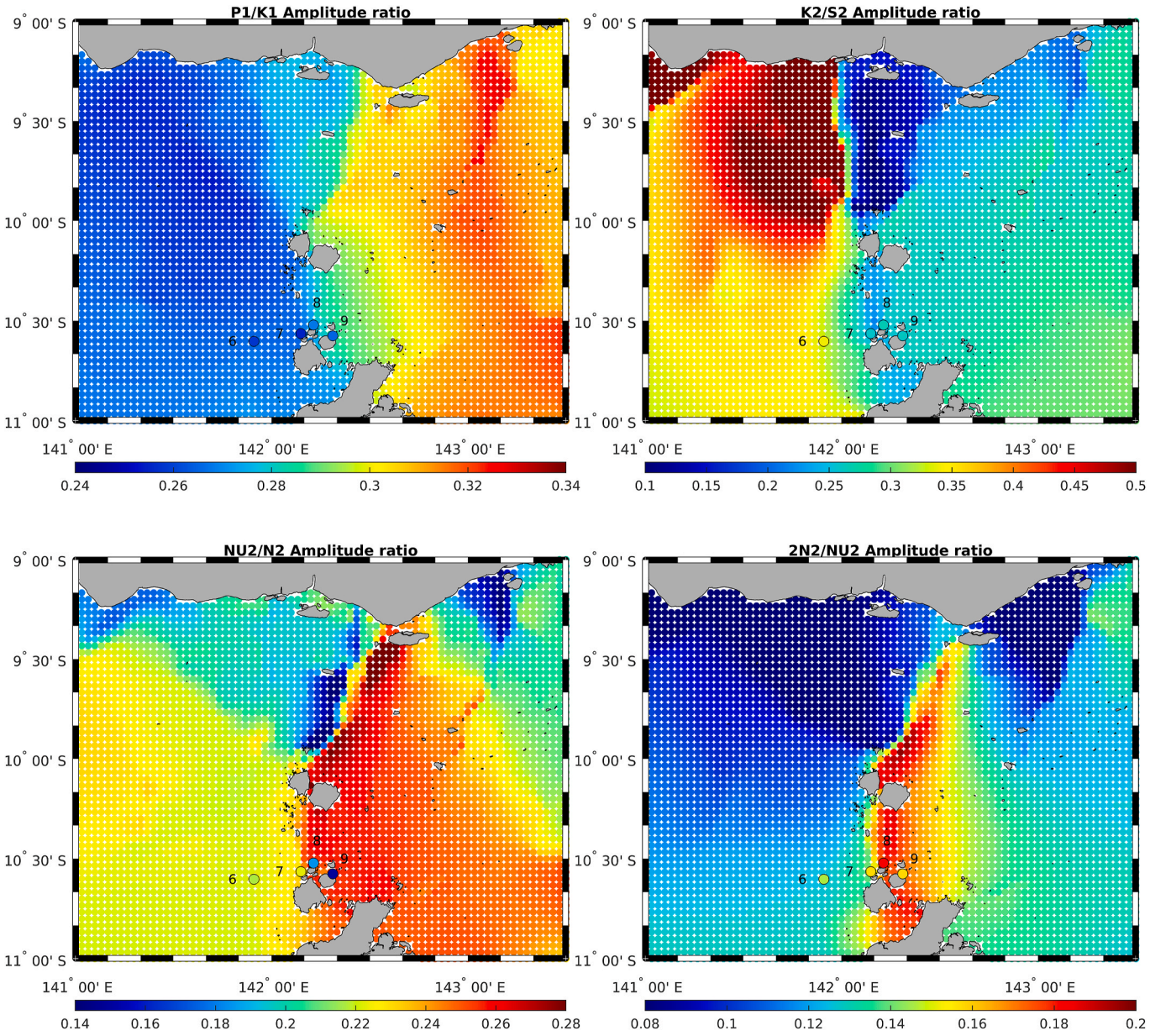

Fig. 3. Empirical amplitude ratios computed from four GESLA3 long tide gauge records in the Torres Strait (numbered circles) plotted on top of the same ratios from FES2022b.

and 4. However, caution should be exercised in some locations and for certain constituents; for instance, in the Torres Strait and also northwest Australia regions for the diurnal ratio P1/K1 where there is a strongly semi-diurnal tidal regime. Further to this, it can be concluded that FES2022b models the amplitude ratio and phase lag differences as well (or better) than the Equilibrium relationships at some locations for some constituents, but caution should be exercised in complex regions such as the Torres Strait and northeastern PNG, as demonstrated in Figs. 2–4.

3.2. *Statistical comparisons of tidal constants from 35-day and long tide gauge records*

Firstly, we evaluate the significance of the amplitude uncertainty in relation to the magnitude of the amplitude for each constituent. RMS is computed as per Eq. (3) from differences between the amplitude for 35-day segments (using only empirical inference ratios and phase lags) and those from the long tide gauge record. This RMS value is used as a proxy for the uncertainty, from which the uncertainty percent σ_P is computed as

$$\sigma_P = (RMS / A_L) \times 100 \quad (4)$$

where A_L is the amplitude of the long tide gauge record. Fig. 5 shows σ_P computed for each constituent amplitude at all 14 tide gauges. This comparison is shown to highlight that where the RMS is similar magnitude to the amplitude, the RMS is misleading. In a case like this, σ_P will be ~100 % and the RMS (uncertainty) calculated for that constituent amplitude is not significant and therefore not useful in this analysis. Only reference constituents were included in Fig. 5, because their related amplitudes showed the same σ_P.

Fig. 5 shows σ_P for six constituents at all 14 tide gauges. As an arbitrary threshold, any constituents with $\sigma_P > 50$ % at any tide gauges were not included in the statistical analysis. This led naturally to the six main constituents shown in Fig. 5. We also compared constituents MS4, MN4, M4 and MM but their σ_P was too large (mostly >50 %) at most tide gauges to justify including them in this uncertainty analysis. The apparent M2 σ_P (red circles) outlier (38 %) at tide gauge 14 (Rabaul) is a

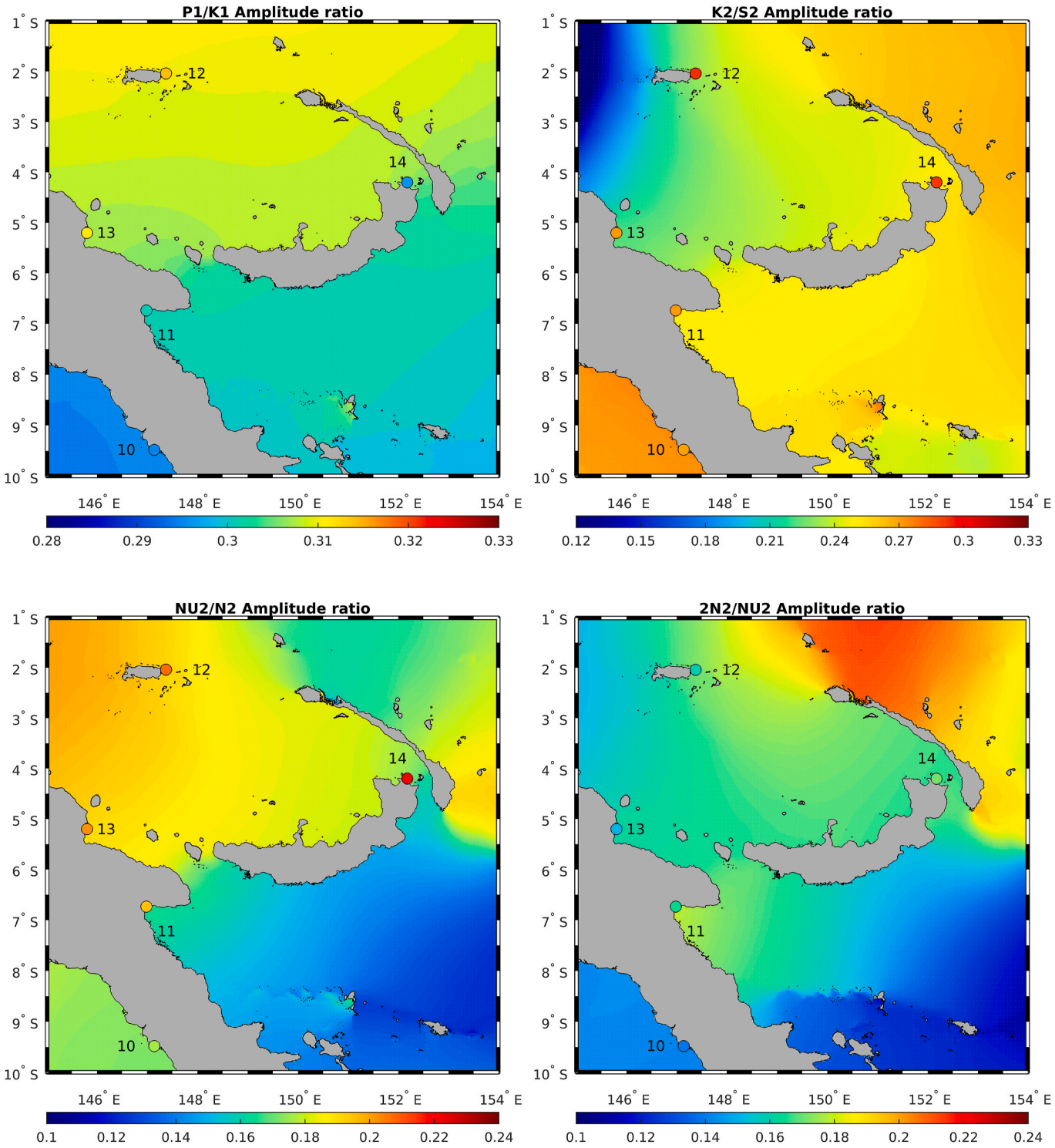

Fig. 4. Empirical amplitude ratios computed from four GESLA3 long tide gauge records around Papua New Guinea (numbered circles) plotted on top of the same ratios from FES2022b.

function of the small M2 amplitude, which in the diurnal tide region of N PNG is 0.035 m. This simply means that with an M2 uncertainty of 0.014 m at Rabaul, M2 σ_P is higher than for other tide gauges with comparatively larger amplitudes.

The descriptive statistics for the differences among the amplitudes computed from the 35-day records and long record at the same tide gauge are shown in Figs. 6–8. These demonstrate the maximum and minimum errors that may be obtained from 35-day tide gauge records compared to the long tide gauge record. We have computed both standard deviation (SD) and RMS of the differences and suggest that the RMS is the best representation of uncertainties for a 35-day tide gauge record as it takes into account any bias in the mean difference. For this reason, and to avoid over-complicating the plots, we show only minimum, maximum, mean and RMS in Figs. 6–8. We show the statistics for the amplitudes computed using the empirical ratios, and the Equilibrium relationships. The results using the empirical amplitude ratios and phase lag differences are tabulated in Appendix 3 (Tables A.3a, A.3b, A.3c) and Appendix 4 (Tables A.4a, A.4b, A.4c). In many cases there is no

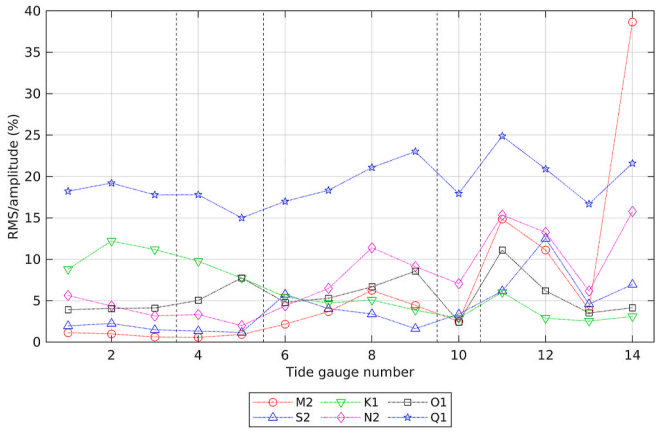

Fig. 5. Shows the RMS of amplitude differences between short 35-day and long tide gauge records as a mean percentage of the amplitude from the long record as computed in Eq. (4). Tide gauge number is according to Table 2. The related constituent amplitudes are the same as their reference constituent in terms of RMS percentage of amplitude (σ_P), so are not plotted here. Vertical dashed lines separate the different regions, as per Table 1.

difference between the different inference approach (i.e. Equilibrium relationships or empirical ratios) but for some reference constituents, notably S2 and K1 for tide gauges 5–9 (NW and TS region) and related constituents such as K2, 2N2 and P1 there are significant differences. The M2 results show that the maximum error from a 35-day record is ~0.07 m at tide gauge 8 (Turtle Head) with tide gauge 6 (Booby Island) and 7 (Goods Island) the next largest at around 0.06 m. The largest minimum error was −0.05 m at tide gauge 5 (Darwin). The maximum RMS is ~0.02 m at tide gauges 7 (Goods Island) and 8 (Turtle Head). The RMS is used as a proxy for the uncertainty in 35-day tide gauges and for the M2 amplitude this is 0.02 m or less for the regions among the 14 tide gauges we evaluated.

Analysing the S2 amplitude errors is more complex. This showed a maximum error in a 35-day tide gauge record of 0.09 m which is at tide gauge 4 (Broome) when using the empirical ratios. In contrast, the minimum error was −0.08 m when using the Equilibrium relationships, also at the Broome tide gauge. From tide gauge 5 (Darwin) to tide gauge 9 (Ince Point), the amplitudes using the empirical inference data were better than those from the Equilibrium relationships by 0.01–0.02 m in maximum and minimum and up to 0.01 m for the RMS. The differences were negligible for tide gauges 10–14 in the PNG region. These results suggested that the empirical inference data is more important in the tidal gradients through the shallow waters of the Torres Strait. This extends to the large phase lag differences in Table 4 for K2/S2 (also see Fig. 2) through the Torres Strait which reach 27.5° at Booby Island, and to the northern PNG region reaching 14.9° at Lombrum-Manus. Adopting the RMS as the S2 uncertainty for the S2 35-day records, we can see that these have a maximum of ~0.01 m for the empirical ratios and ~0.02 for the Equilibrium relationships in the Torres Strait. The N2 amplitude statistics in Fig. 6 indicate the maximum RMS of 0.01 m at tide gauge 8 (Turtle Head), with maximum and minimum difference of +0.05 m and −0.04 m at this same location. There are some differences among the results from the empirical ratio compared to when the Equilibrium relationships were used, but these all appear to be ~0.01 m or less.

Fig. 7 shows the statistics of the differences for 35-day records for three diurnal constituent amplitudes. These are K1, O1, and Q1. The K1 amplitude is perhaps the most problematic, compounded by the differences between using the empirical inference or Equilibrium relationships. When using empirical inference, the 35-day record has RMS reaching ~0.05 m at tide gauge 5 (Darwin). The K1 maximum amplitude differences are up to 0.09 m at tide gauges 5–8 (Darwin to Turtle Head), indicating that the north west and Torres Strait regions can have 35-day records that may be in error up to 0.09 m compared to the K1 amplitude from the long tide gauge record when using empirical inference values. The O1 maximum is 0.07 m at tide gauge 5 (Darwin) with the minimum −0.08 m at tide gauge 11 (Lae), noting that the Lae tide gauge record is only 3.5 years long, and plots (not shown here) suggest the final 35-day record may be an outlier for the diurnal tides and have biased these results. The O1 RMS is around 0.02 m for tide gauges 5–9, which is Darwin and the Torres Strait tide gauges. The Q1 amplitude maximum reaches almost 0.05 m at tide gauge 7 (Goods Island) with the minimum of ~ -0.03 m at tide gauge 6 (Booby Island) and tide gauge 8 (Turtle Head).

The K2 results in Fig. 8 show similar characteristics to S2, which is expected, given that K2 is related to the reference constituent S2. The maximum difference is ~0.03 m at tide gauge 4 (Broome), but as with S2, this is when using the empirical inference information. Notably, the minimum is nearly −0.04 m, but this is when the Equilibrium relationships are used. This appears to show that although there is no obviously better result from the maximum and minimum, the mean from the Equilibrium relationships is biased negatively by ~0.015 m at Broome and ~0.01 m at tide gauges 3, 5, 6 (west and north west region) whereas the mean when using the empirical inference is close to zero. The RMS for the results using the empirical inference is smaller by up to 0.01 m at these tide gauges. There also appear to be larger differences at Torres Strait tide gauge 6 (Booby Island), 8 (Turtle Head) and 9 (Ince Point).

The 2N2 amplitude statistics indicate much smaller RMS from the empirical inference. The mean is close to zero and the RMS is generally only 0.001 m–0.002 m, peaking at ~0.005 m at tide gauge 8 (Turtle Head) where the maximum and minimum are about ±0.01 m. This can be considered in terms of 2N2 amplitudes of 0.024 m at Turtle Head, reaching 0.077 m at Broome. In contrast, the Equilibrium relationships show means of up to 0.01 m at Broome, with maximum at this tide gauge of 0.02 m. The P1 amplitude is the related constituent to K1 and it is apparent that the differences where the empirical inference is used have resulted in smaller errors in the 35-day records. When the Equilibrium relationships are used, the mean increases in the northwest region (tide gauges 4 and 5), increasing to 0.04–0.05 m through the Torres Strait. In contrast, the mean for the differences using the empirical inference is close to zero for all tide gauges. The big differences among the RMS for the Equilibrium relationships (red diamonds) and the empirical ratios (black diamonds) are significant. The RMS from the empirical inference is 0.01 m or less, while those from the Equilibrium relationships reach 0.05 m through the Torres Strait, with maximum error up to 0.09 m.

3.3. Amplitude and phase lag differences

This section shows time series of differences in amplitude for the 35-day records (only using the empirical inference ratios and phase lags) compared to those from the long record (all 19-years in length) for four tide gauges, representing the west region (tide gauge 2, Onslow Beadon Creek; 2000–2019), the northwest region (tide gauge 4, Darwin; 2000–2019), Torres Strait region (tide gauge 8, Turtle Head; 2000–2019) and the northern PNG region (tide gauge 14, Rabaul; 1975–1994). Port Moresby is the only tide gauge in the south east PNG region, but we chose not to show it here because it is not a full 19 year record, and because the magnitude of its amplitude was similar to other regions. Fig. 9 shows amplitudes for three semi-diurnal constituents (M2, S2 and N2), with two diurnal constituents (K1 and O1) in Fig. 10, and three related constituents (K2, 2N2 and P1) in Fig. 11. These demonstrate the characteristics in the different regions and among the different constituents and how the 35-day constituents may vary compared to those from the long records. We refer to Appendix 3 for the RMS, maximum and minimum values for these plots. Note that most time series in Figs. 9–11 have been vertically offset to their actual amplitude on the y-axis so they can be clearly seen within one plot with the y-axis limited to a maximum of 0.5 m so that the amplitude

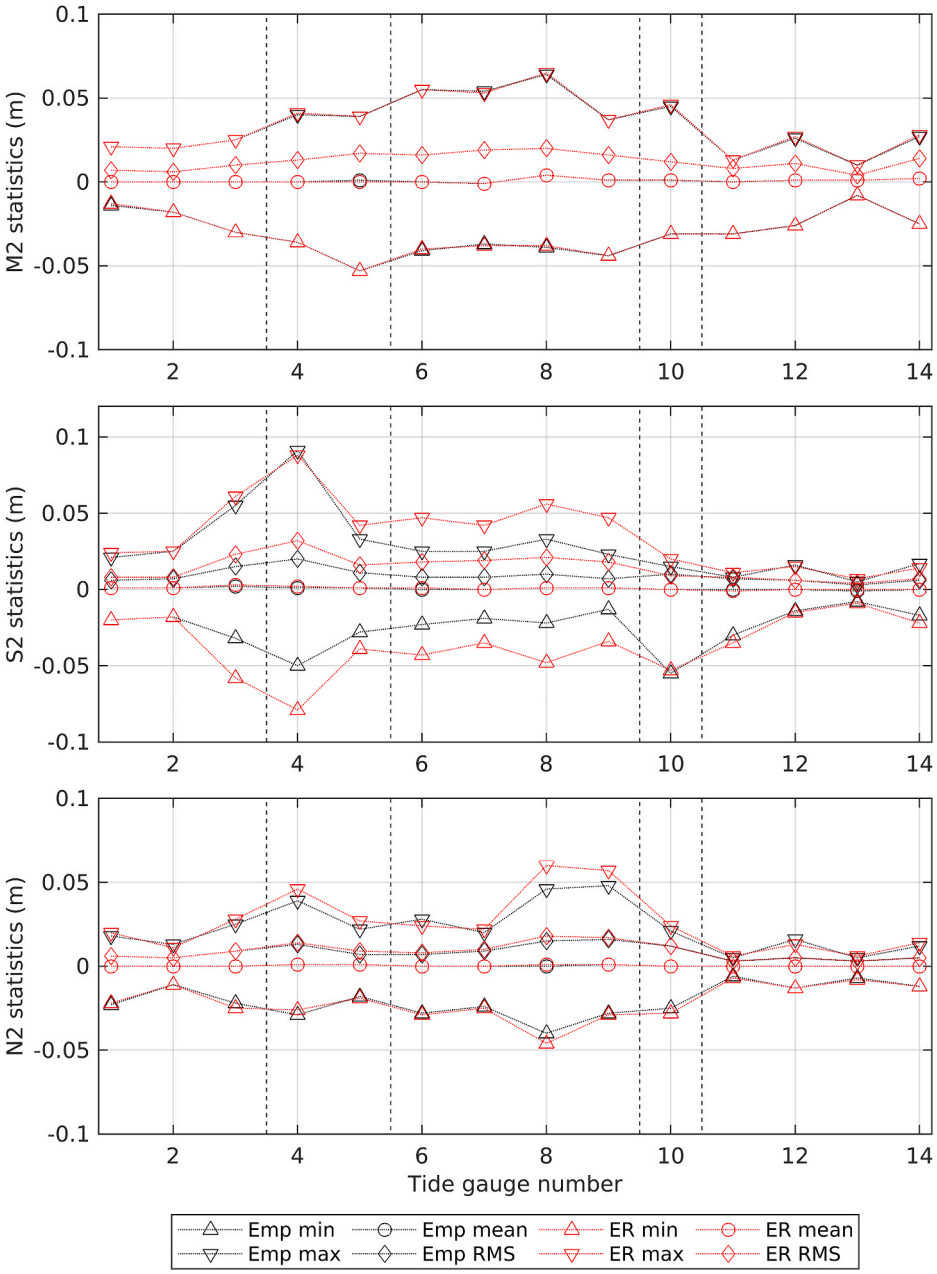

Fig. 6. Shows the descriptive statistics of the differences between amplitudes for M2, S2 and N2 from 35-day and long tide gauge records at 14 tide gauges. Tide gauge number is according to Table 2. Differences when using eight empirical ratios and phase lag differences for the inferred constituents are in black, with the eight equilibrium relationships in red, with each statistic as per the legend. Vertical dashed lines separate the different regions, as per Table 2. (For interpretation of the references to colour in this figure legend, the reader is referred to the Web version of this article.)

differences can be directly compared. The actual amplitudes are shown in Table A.1. The 'years' label on the x-axis refers to the 19-year record starting from January 2000 for Onslow Beadon Creek, Darwin and Turtle Head, but from January 1975 for Rabaul.

In Fig. 9, the 35-day M2 amplitude at Darwin (magnitude 1.851 m in Table A.1) has differences reaching 0.050 m and −0.040 m (Appendix 3) compared to the long record. There appears to be a periodic signal, although it is variable from year to year. Onslow Beadon Creek has relatively small M2 maximum and minimum differences compared to the long record of ±0.02 m. It shows only small variations in time with a small periodic signal and occasional variations. On the other hand, tide gauge 8 at Turtle Head in the Torres Strait has much larger differences, reaching +0.060 m and −0.040 m respectively. The time series indicates a periodic signal with the maximum occurring annually during the months November to March, which approximately aligns with the austral summer and northern Australian wet season. The amplitude varies over time, which is most noticeable over the last third of the record, where the magnitude of the periodic signal becomes much smaller. There is some periodicity in the M2 amplitude difference for tide gauge 14 (Rabaul) although its character varies over the full record.

The S2 35-day differences at Darwin have slightly smaller maximum (0.033 m) and minimum (−0.028 m) than the M2. The differences for S2 at Onslow Beadon Creek are very similar to those for M2, with Turtle Head S2 differences smaller and less variable than for M2 (RMS 0.01 m, maximum 0.033 m and minimum −0.022 m). The S2 differences at Rabaul are also less than those for M2, despite the S2 amplitude being double the M2 amplitude at Rabaul (0.035 m–0.086 m). The N2 differences are more distinct. At Darwin there is a weak long period signal

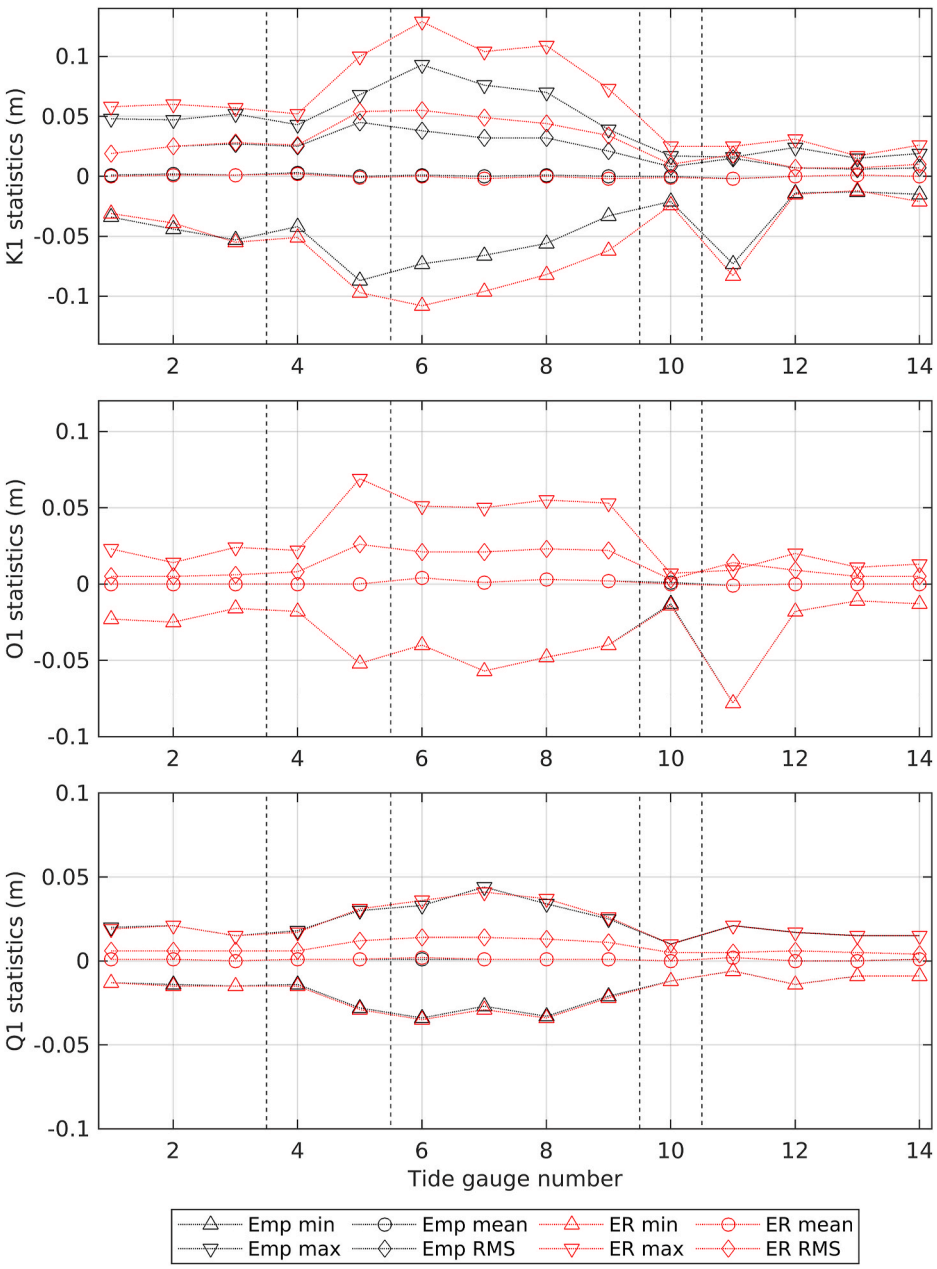

Fig. 7. Shows the descriptive statistics of the differences among amplitudes for K1, O1, and Q1 from 35 day and long tide gauge records at 14 tide gauges. Tide gauge number is according to Table 2. Differences when using eight empirical ratios and phase lag differences for the inferred constituents are in black, with the eight equilibrium relationships in red, with each statistic as per the legend. Vertical dashed lines separate the different regions, as per Table 2. (For interpretation of the references to colour in this figure legend, the reader is referred to the Web version of this article.)

which is probably attributable to the 8.85-year perigean cycle (e.g., Feng et al., 2015). This perigean cycle is also apparent in the Turtle Head N2 differences, although it has a different phase. The N2 differences at Turtle Head also appear much noisier, with an apparent seasonal signal, although inconsistent in amplitude. Onslow Beadon Creek also shows the perigean cycle, albeit with a much smaller amplitude but approximately in phase with Darwin. The perigean cycle is barely discernible at Rabaul.

Fig. 10 shows the diurnal tidal constituents K1 and O1 for the four tide gauge records. The K1 amplitude time series of differences for Turtle Head shows a strong annual signal (maximum coinciding with the austral summer) of ~0.05 m, but with a 5–6 year period (~2003–2009) of slightly smaller annual amplitude and apparently negative bias to the long record amplitude. It is not clear what may have caused this. The K1 differences at Darwin show a large annual signal, with maximum 0.068 m, minimum −0.087 m. Rabaul has a small K1 annual signal with maximum 0.019 m and minimum −0.015 m. In contrast, Onslow Beadon Creek has a smaller amplitude, but larger annual signal reaching ~ ±0.045 m, so that its σ_P value (Eq. (4)) in Fig. 5 reaches ~12 %. The reasons for the pronounced annual periodic signal in the K1 35-day amplitude in the Torres Strait, north west, and west region are not clear but are assumed to be connected to the distinct seasonal variations across northern Australia. The northern Australian 'wet' season runs from October to April, and features higher rainfall and temperatures combined with lower atmospheric pressure, while the 'dry 'season runs from May to September and has lower rainfall and temperatures but higher atmospheric pressure. The K1 periodic highs appear to correlate with the wet season and the lows to the dry season, suggesting that these seasonal atmospheric conditions contribute to this pronounced signal. It is possible that the shallow bathymetry in the Torres Strait, and complex

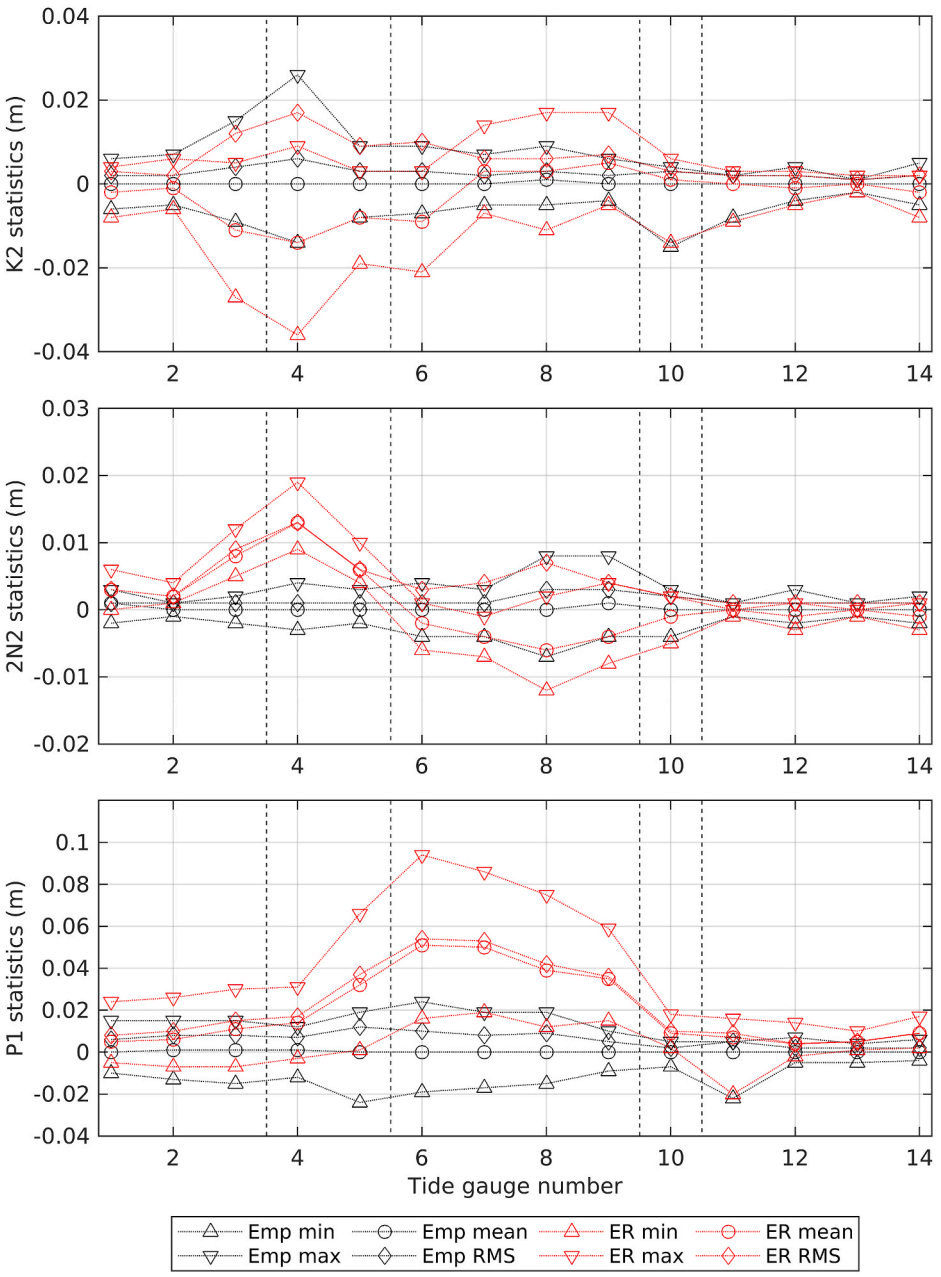

Fig. 8. Shows the descriptive statistics of the differences among amplitudes for K2, 2N2, and P1 from 35 day and long tide gauge records at 14 tide gauges. Tide gauge number is according to Table 2. Differences when using eight empirical ratios and phase lag differences for the inferred constituents are in black, with the eight Equilibrium relationships in red, with each statistic as per the legend. Vertical dashed lines separate the different regions, as per Table 2. (For interpretation of the references to colour in this figure legend, the reader is referred to the Web version of this article.)

coastal characteristics specific to each region may also contribute to this signal and its spatial variation, but further investigation would be needed to better understand this.

The O1 amplitude differences at Turtle Head show similar characteristics to K1, but with a strong annual and semi-annual signal. The amplitude of this periodic signal also appears to be reduced through the 2003–2009 period at this tide gauge, as for K1. This is similar to other Torres Strait tide gauges plotted (but not shown here), suggesting an atmospheric event over this time period in this region. The O1 amplitude differences at Darwin are also large, with maximum 0.069 m and minimum −0.052 m. Fig. 11 shows the 35-day record amplitude differences for the related constituents K2, 2N2 and P1. K2 is related to S2 and shows good agreement, demonstrating that with accurate inference information, the K2 constituents can be accurately resolved from 35-day tide gauge records. The 2N2 amplitude differences for Turtle Head clearly show the perigean cycle, perhaps as expected given that it is the related constituent for N2 which also showed this. The y-axis scale should be noted, as these differences are quite small with the 2N2 maximum differences no more than 0.01 m at Turtle Head and only about 0.003 m at other tide gauges. The perigean cycle can be seen at Darwin, although with an amplitude of ~0.001 m. P1 is also related to K1 and shows the same characteristics, with a well defined annual signal at Onslow Beadon Creek, Darwin and Turtle Head. Rabaul also has this signal, but with a very small annual error compared to the long tide gauge amplitude.

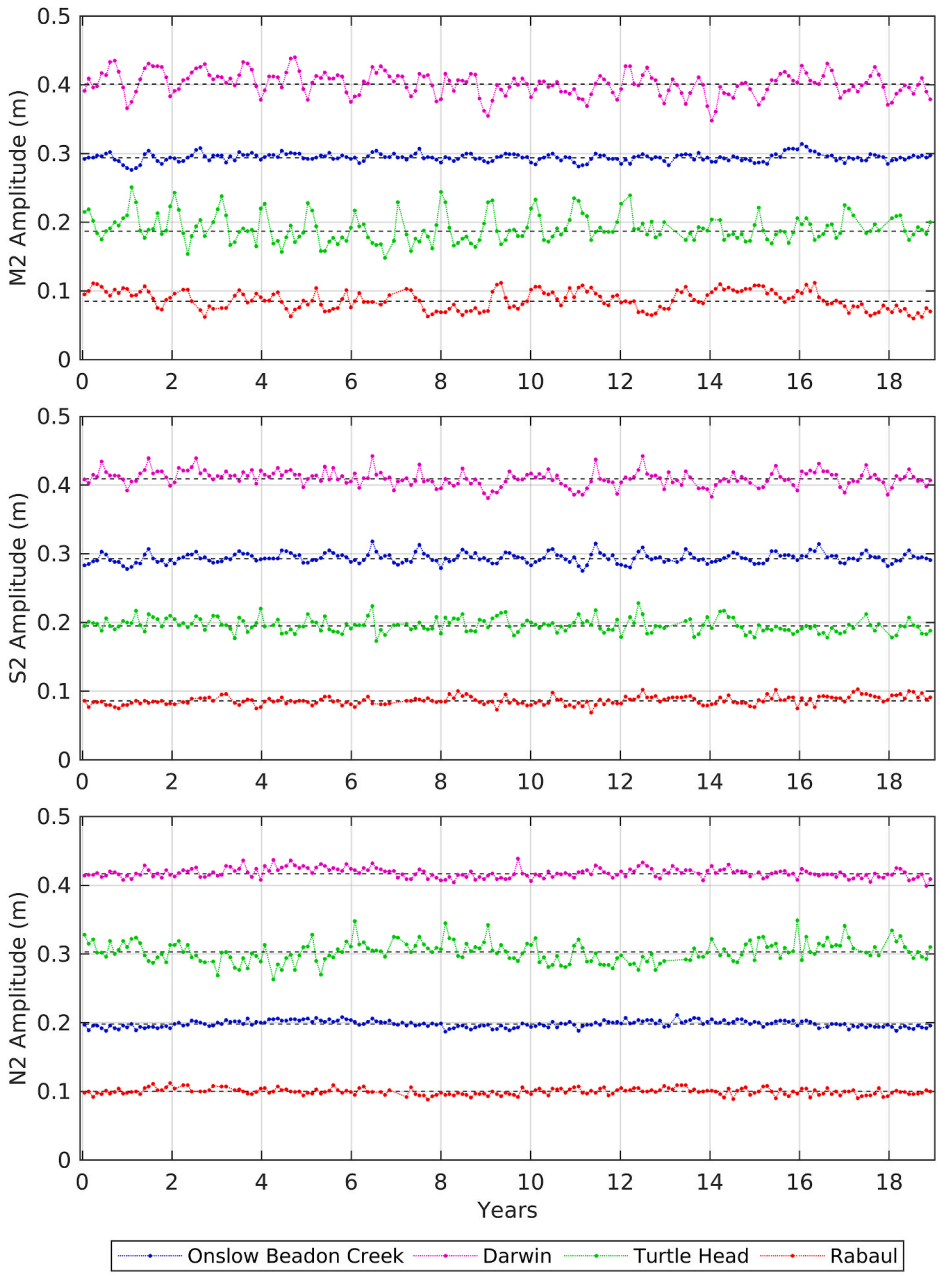

Fig. 9. M2, S2 and N2 35-day amplitudes compared to the 19 year amplitude for each (black dashed lines). These are shown for four representative tide gauges as per the legend. Amplitudes have been offset vertically (but still ranked from largest to smallest amplitude for each constituent) on the y-axis so all time series can be viewed on one plot (see Table A.1 for actual amplitudes). The x-axis shows the 19 year record from the start of each record, which is January 2000 for all tide gauges except Rabaul which starts in January 1975.

4. Conclusions

We have analysed the uncertainties associated with nine constituents from 35-day tide gauge records compared to the nine long record constituents from the same 14 tide gauges across the northern Australian and PNG regions. Those constituents analysed comprise six reference constituents (M2, S2, N2, K1, O1, Q1) and three related constituents (K2, 2N2, P1) which were chosen because their uncertainties were significant in comparison to their amplitudes as shown in Fig. 5.

Empirical amplitude ratios and phase lag differences for eight related constituents were compared to the relationships based on the Equilibrium tide so as to identify constituent or location-dependent variability in accuracy. The largest differences in the amplitude ratios were for P1/K1, where Fig. 2 shows all tide gauge empirical amplitude ratios were less than the 0.331 value, and also lower than the revised P1/K1 amplitude ratio of 0.318 from Ray (2017). The Torres Strait region showed the largest differences between the empirical amplitude ratios and the Equilibrium relationships, also highlighted in Figs. 2, and Figs. 6–8. There were also large phase lag differences between the empirical and Equilibrium relationships (the latter being all zero), again mostly in the Torres Strait (Fig. 2) which suggests that accurate inference is dependent on the empirical phase lag differences as well as the amplitude ratio. Our results (using FES2022b as an example) also suggested that OTM-derived amplitude ratios and phase lag differences could be used as inference information for short records in some instances.

We adopted the RMS as a proxy for the 35-day record uncertainty for each amplitude for the different regions which are shown in Figs. 6–8

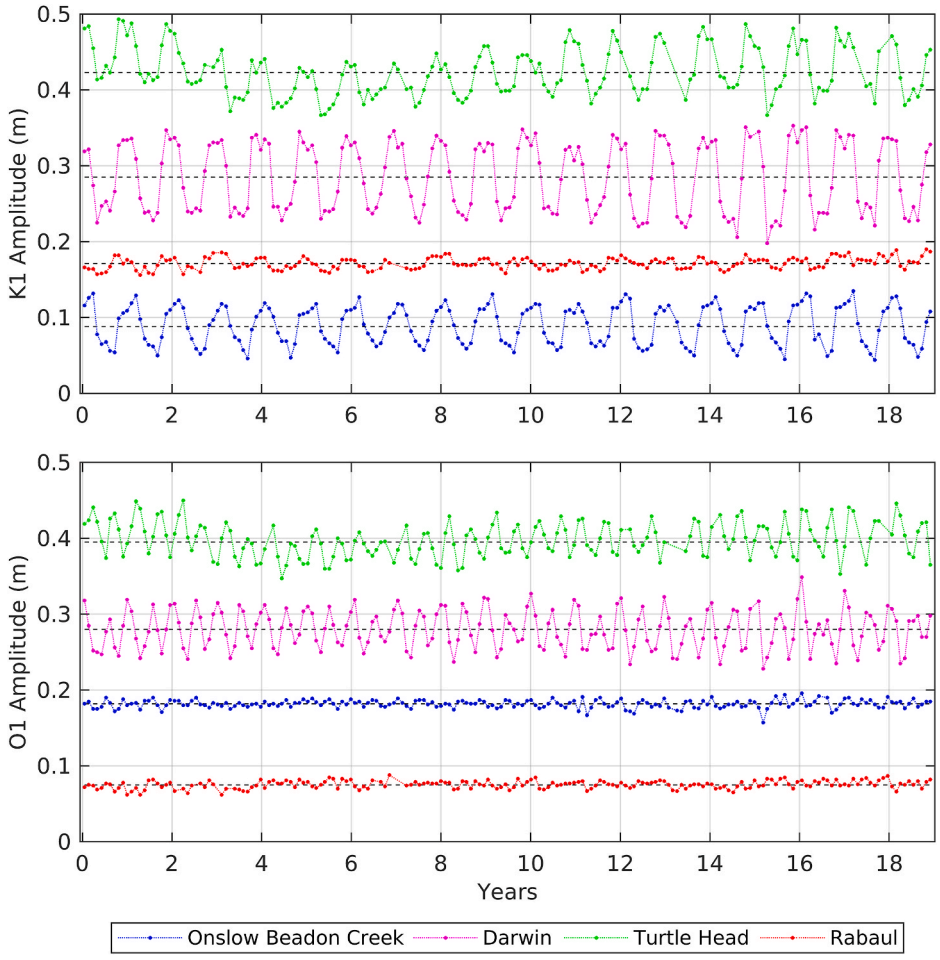

Fig. 10. K1 and O1 35-day amplitudes (coloured dots) compared to the 19-year amplitude for each (black dashed line). These are shown for four representative tide gauges as per the legend. Amplitudes have been offset vertically on the y-axis (but still ranked from largest to smallest amplitude for each constituent) so all time series can be viewed on one plot (see Table A.1 for actual amplitudes). The x-axis shows the 19 year record from the start of each record, which is January 2000 for all tide gauges except Rabaul which starts in January 1975.

and in Appendix 3 (Tables A.3a, A.3b, A.3c). This suggested smaller uncertainty in the west (maximum RMS = 0.027 m for K1) and N PNG (maximum RMS = 0.015 m for K1) regions and largest uncertainty in the north west (maximum RMS = 0.045 m for K1) and Torres Strait (maximum RMS = 0.038 m for K1) regions. This applied to most constituents, but most noticeably to the diurnal constituents. The empirical inference information showed improved statistics for S2 and K1 and their related constituents K2, 2N2 and P1, mostly in the northwest and Torres Strait regions. This improvement was no more than 0.02 m in RMS but was as much as 0.07 m for the P1 maximum 35-day error in the Torres Strait. The maximum errors (using only empirical inference) for the 35-day records tended to relate to annual or semi-annual periodic variation and reached errors of 0.091 m (S2, north west) and 0.093 m (K1, Torres Strait) which indicate an upper bound for 35-day record errors. These could be seen in the 35-day time series in Figs. 9–11, with diurnal tides K1 and O1 showing a strong annual signal, with apparent periodic modulation of the signal. This annual signal was strongest for K1 in the west, northwest and Torres Strait regions and appears to coincide with the austral summer months, which is also the wet season in Australia's north.

Our results suggest that the AHO short tide gauge records (35-days) can be used in tidal studies near or at the coast in these regions to estimate six reference constituents to uncertainties of less than 0.045 m with maximum errors not exceeding 0.093 m. These are upper bound errors and are generally much less depending on constituents and location. It is important to qualify that these uncertainty estimates relate to the location of the long tide gauge records used in the study. Hence, these uncertainties will increase if used for short tide gauge records at large distances from the reference tide gauge, although this increase is dependent on the changed bathymetric and other conditions at the distant short tide gauge. Three related constituents (K2, 2N2, P1) can be estimated from the 35-day records to an uncertainty not exceeding 0.010 m and maximum of 0.024 m or less provided that accurate empirical inference information can be obtained from a long record, or

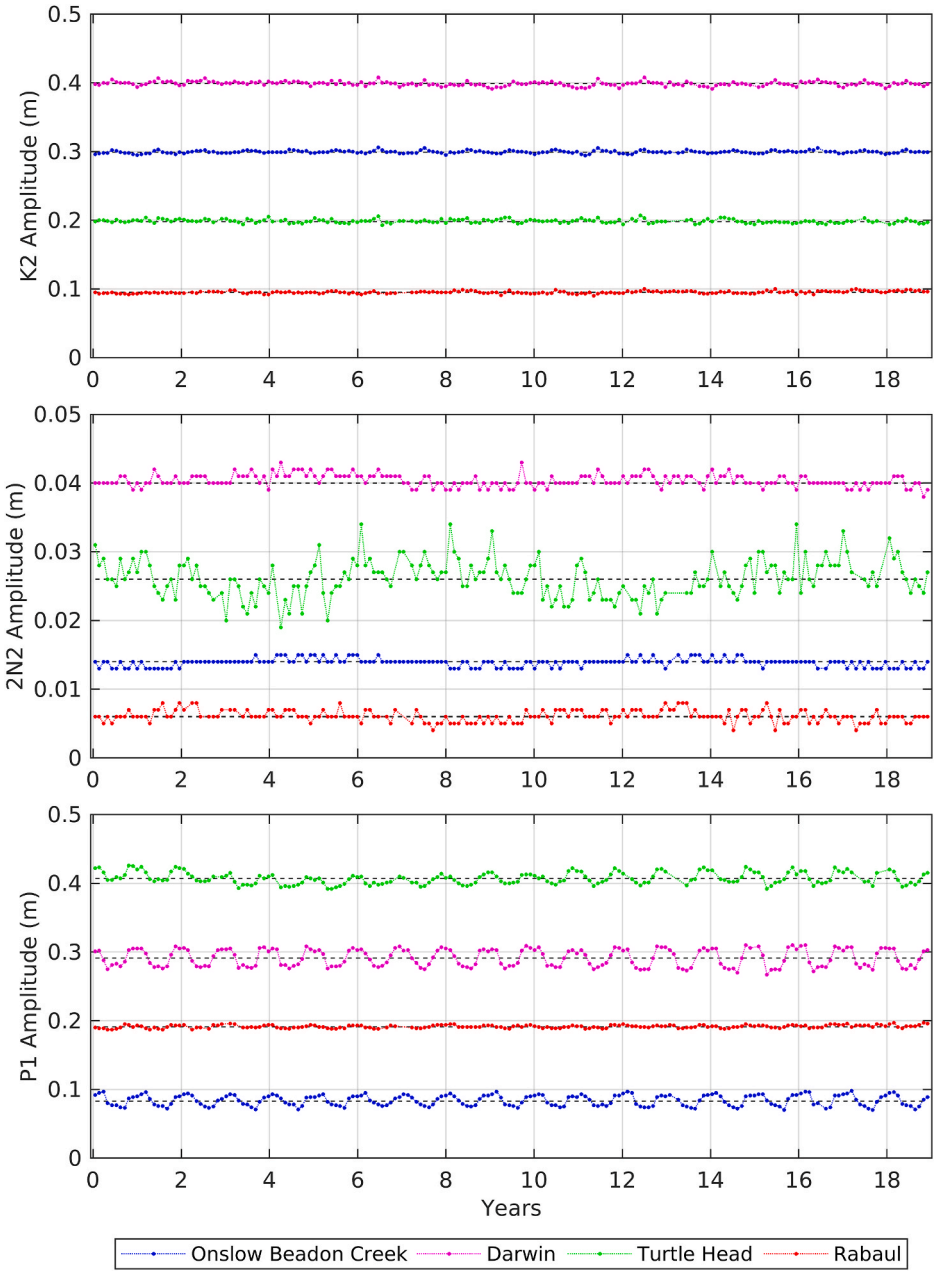

Fig. 11. K2, 2N2 and P1 35-day amplitudes compared to the 19-year amplitude for each (black dashed line) shown for four representative tide gauges as per the legend. Amplitudes have been offset vertically on the y-axis (but still ranked from largest to smallest amplitude for each constituent) so all time series can be viewed on one plot (see Table A.1 for actual amplitudes). The x-axis shows the 19-year record from the start of each record, which is January 2000 for all tide gauges except Rabaul which starts in January 1975.

in some instances an OTM. These uncertainties should be considered as reasonable accuracy limits for the use of short tide gauge records in this region for a range of tidal studies.

CRediT authorship contribution statement

M.S. Filmer: Writing – review & editing, Writing – original draft, Methodology, Investigation, Formal analysis, Conceptualization. **P.L. Woodworth:** Writing – review & editing, Methodology, Conceptualization. **S.D.P. Williams:** Writing – review & editing, Methodology, Conceptualization. **S.J. Claessens:** Writing – review & editing, Methodology, Investigation.

Data statement

Short tide gauge records are available on request from the Australian Hydrographic Office.

FES2022b is available from https://www.aviso.altimetry.fr/en/data/products/auxiliary-products/global-tide-fes.html.

GESLA3 dataset is available from https://gesla787883612.wordpress.com/downloads/

Funding sources

A component of this research was supported by The Australian Hydrographic Office, Department of Defence under Grant FSI-4002.

Declaration of competing interest

The authors declare the following financial interests/personal relationships which may be considered as potential competing interests. Mick Filmer reports financial support was provided by Australian Hydrographic Office. Mick Filmer reports a relationship with Australian Hydrographic Office that includes: funding grants. If there are other authors, they declare that they have no known competing financial interests or personal relationships that could have appeared to influence the work reported in this paper.

Acknowledgements

We would like to thank AVISO for FES2022b, the GESLA Team and contributors for the GESLA3 dataset, and Daniel L. Codiga for the UTide MATLAB Software.

"The FES2022 Tide product was funded by CNES, produced by LEGOS, NOVELTIS and CLS and made freely available by AVISO". CNES, 2024. FES2022 (Finite Element Solution) Ocean Tide (Version 2022) [Data set]. CNES. https://doi.org/10.24400/527896/A01-2024.00.

The authors would also like to thank the Australian Hydrographic Office for supplying the locations of the short tide gauge data for this study under licence and subject to the following conditions. "Certain material in this product is reproduced under licence by permission of The Australian Hydrographic Office. © Commonwealth of Australia 2022). All rights reserved."

Fig. 1 was plotted using the Generic Mapping Tools (Wessel et al., 2013). The authors thank the editor and reviewers for their constructive comments which have helped us to improve the manuscript.

APPENDIX 1

Table A.1
Amplitudes from long tide gauge records (metres)

Tide gauge site	M2	S2	K2	K1	P1	O1	Q1	N2	2N2	NU2	T2
Exmouth	0.581	0.308	0.086	0.212	0.065	0.137	0.031	0.106	0.011	0.020	0.015
Onslow Beadon Creek	0.594	0.323	0.089	0.208	0.063	0.132	0.030	0.108	0.012	0.021	0.018
Port Hedland	1.701	1.031	0.292	0.242	0.069	0.149	0.034	0.289	0.030	0.057	0.052
Broome	2.381	1.479	0.417	0.256	0.071	0.158	0.036	0.398	0.040	0.077	0.074
Darwin	1.851	0.959	0.269	0.585	0.161	0.330	0.077	0.347	0.040	0.066	0.052
Booby Island	0.722	0.142	0.048	0.702	0.181	0.430	0.081	0.170	0.025	0.037	0.007
Goods Island	0.527	0.201	0.052	0.677	0.173	0.398	0.075	0.138	0.022	0.031	0.010
Turtle Head	0.327	0.295	0.078	0.623	0.167	0.345	0.063	0.133	0.024	0.024	0.022
Ince Point	0.369	0.413	0.108	0.532	0.141	0.262	0.047	0.174	0.027	0.026	0.024
Port Moresby	0.486	0.286	0.077	0.280	0.083	0.141	0.027	0.165	0.023	0.029	0.021
Lae	0.056	0.107	0.029	0.247	0.074	0.130	0.021	0.020	0.003	0.004	0.011
Lombrum Manus Island	0.099	0.047	0.014	0.234	0.074	0.146	0.027	0.039	0.006	0.008	0.004
Madang	0.095	0.060	0.016	0.243	0.076	0.144	0.028	0.042	0.006	0.008	0.005
Rabaul	0.035	0.086	0.025	0.241	0.071	0.125	0.020	0.030	0.005	0.007	0.008

APPENDIX 2

Table A.2
Greenwich phase lags from long tide gauge records (degrees)

Tide gauge site	M2	S2	K2	K1	P1	O1	Q1	N2	2N2	NU2	T2
Exmouth	78.956	144.778	142.308	177.093	174.331	167.374	161.427	52.832	18.373	49.510	159.766
Onslow Beadon Creek	69.130	131.837	129.696	172.833	168.860	164.077	159.119	42.899	8.672	45.455	140.040
Port Hedland	74.359	135.413	133.627	172.607	171.372	161.677	154.697	47.411	13.718	47.358	140.898
Broome	65.808	125.690	123.601	171.835	174.013	160.890	153.461	40.198	6.070	38.045	128.292
Darwin	249.252	297.973	295.801	200.438	204.222	190.029	183.785	228.354	203.667	233.756	299.667
Booby Island	203.487	323.305	295.850	44.699	36.965	352.396	328.549	162.678	128.001	169.194	285.640
Goods Island	203.577	2.420	336.853	50.292	41.707	357.713	333.629	153.209	124.281	165.017	326.878
Turtle Head	172.645	31.925	14.147	56.411	49.029	7.159	347.515	119.180	102.742	142.208	27.680
Ince Point	113.268	42.846	32.957	59.182	54.836	10.408	350.740	89.763	82.083	100.605	19.173
Port Moresby	349.536	309.279	306.059	43.532	39.291	13.507	351.526	332.256	324.582	336.878	290.714
Lae	157.467	186.054	177.902	54.133	49.836	30.691	14.122	243.005	205.746	246.655	187.662
Lombrum Manus Island	283.347	155.674	140.728	61.231	61.464	46.765	38.360	248.613	212.284	258.965	167.358
Madang	279.474	177.187	166.853	59.370	57.638	46.073	35.380	253.824	217.430	257.562	188.651
Rabaul	244.641	170.533	161.756	54.810	51.724	34.687	23.198	245.483	202.873	257.446	189.578

APPENDIX 3

Table A.3a
Statistics for amplitude differences between 35-day and long tide gauge records using empirical inference information (metres).

Tide gauge site	M2			S2			N2		
	RMS	MIN	MAX	RMS	MIN	MAX	RMS	MIN	MAX
Exmouth	0.007	−0.014	0.021	0.006	−0.020	0.021	0.006	−0.023	0.018
Onslow Beadon Creek	0.006	−0.018	0.020	0.007	−0.018	0.025	0.005	−0.011	0.013
Port Hedland	0.010	−0.030	0.025	0.015	−0.032	0.055	0.009	−0.022	0.025
Broome	0.013	−0.036	0.040	0.020	−0.050	0.091	0.013	−0.029	0.039
Darwin	0.017	−0.053	0.039	0.011	−0.028	0.033	0.007	−0.018	0.022
Booby Island	0.016	−0.041	0.055	0.008	−0.023	0.025	0.007	−0.028	0.028
Goods Island	0.019	−0.037	0.054	0.008	−0.019	0.025	0.009	−0.024	0.020
Turtle Head	0.020	−0.039	0.064	0.010	−0.022	0.033	0.015	−0.040	0.046
Ince Point	0.016	−0.044	0.037	0.007	−0.013	0.023	0.016	−0.028	0.048
Port Moresby	0.012	−0.031	0.045	0.010	−0.055	0.015	0.012	−0.025	0.021
Lae	0.008	−0.031	0.013	0.007	−0.030	0.008	0.003	−0.006	0.005
Lombrum Manus Island	0.011	−0.026	0.026	0.006	−0.014	0.016	0.005	−0.013	0.016
Madang	0.004	−0.008	0.010	0.003	−0.008	0.005	0.003	−0.007	0.005
Rabaul	0.014	−0.025	0.027	0.006	−0.017	0.017	0.005	−0.012	0.012

Table A.3b:

Tide gauge site	K1			O1			Q1		
	RMS	MIN	MAX	RMS	MIN	MAX	RMS	MIN	MAX
Exmouth	0.019	−0.034	0.048	0.005	−0.023	0.023	0.006	−0.013	0.020
Onslow Beadon Creek	0.025	−0.044	0.047	0.005	−0.025	0.014	0.006	−0.014	0.021
Port Hedland	0.027	−0.053	0.052	0.006	−0.016	0.024	0.006	−0.015	0.015
Broome	0.025	−0.042	0.043	0.008	−0.018	0.022	0.006	−0.014	0.018
Darwin	0.045	−0.087	0.068	0.026	−0.052	0.069	0.012	−0.028	0.030
Booby Island	0.038	−0.073	0.093	0.021	−0.040	0.051	0.014	−0.034	0.033
Goods Island	0.032	−0.066	0.076	0.021	−0.057	0.050	0.014	−0.027	0.044
Turtle Head	0.032	−0.056	0.070	0.023	−0.048	0.055	0.013	−0.033	0.034
Ince Point	0.021	−0.033	0.039	0.022	−0.040	0.053	0.011	−0.021	0.025
Port Moresby	0.008	−0.021	0.017	0.003	−0.013	0.007	0.005	−0.012	0.010
Lae	0.015	−0.073	0.016	0.014	−0.078	0.009	0.005	−0.006	0.021
Lombrum Manus Island	0.007	−0.014	0.024	0.009	−0.018	0.020	0.006	−0.014	0.017
Madang	0.006	−0.013	0.015	0.005	−0.011	0.011	0.005	−0.009	0.015
Rabaul	0.007	−0.015	0.019	0.005	−0.013	0.013	0.004	−0.009	0.015

Table A.3c:

Tide gauge site	K2			P1			2N2		
	RMS	MIN	MAX	RMS	MIN	MAX	RMS	MIN	MAX
Exmouth	0.002	−0.006	0.006	0.006	−0.010	0.015	0.001	−0.002	0.003
Onslow Beadon Creek	0.002	−0.005	0.007	0.008	−0.013	0.015	0.001	−0.001	0.001
Port Hedland	0.004	−0.009	0.015	0.008	−0.015	0.015	0.001	−0.002	0.002
Broome	0.006	−0.014	0.026	0.007	−0.012	0.012	0.001	−0.003	0.004
Darwin	0.003	−0.008	0.009	0.012	−0.024	0.019	0.001	−0.002	0.003
Booby Island	0.003	−0.007	0.009	0.010	−0.019	0.024	0.001	−0.004	0.004
Goods Island	0.002	−0.005	0.007	0.008	−0.017	0.019	0.001	−0.004	0.003
Turtle Head	0.003	−0.005	0.009	0.009	−0.015	0.019	0.003	−0.007	0.008
Ince Point	0.002	−0.004	0.006	0.005	−0.009	0.010	0.003	−0.004	0.008
Port Moresby	0.003	−0.015	0.004	0.002	−0.007	0.005	0.002	−0.004	0.003
Lae	0.002	−0.008	0.002	0.005	−0.022	0.005	0.001	−0.001	0.001
Lombrum Manus Island	0.002	−0.004	0.004	0.002	−0.005	0.007	0.001	−0.002	0.003
Madang	0.001	−0.002	0.001	0.002	−0.005	0.004	0.001	−0.001	0.001
Rabaul	0.002	−0.005	0.005	0.002	−0.004	0.006	0.001	−0.002	0.002

APPENDIX 4

Table A.4a
Statistics for phase lag differences between 35-day and long tide gauge records using empirical inference information (degrees).

Tide gauge site	M2			S2			N2		
	RMS	MIN	MAX	RMS	MIN	MAX	RMS	MIN	MAX
Exmouth	1.660	−4.091	7.560	1.761	−4.532	6.905	3.329	−6.414	14.078
Onslow Beadon Creek	0.709	−1.400	3.735	1.220	−2.259	3.004	2.357	−6.334	7.329
Port Hedland	0.649	−1.845	1.789	0.977	−2.150	2.319	2.011	−3.779	4.867
Broome	0.766	−1.865	1.714	0.833	−1.934	1.951	1.818	−4.089	5.098
Darwin	0.713	−3.248	1.430	0.807	−3.393	1.734	1.519	−4.087	3.659
Booby Island	2.402	−6.170	5.883	2.999	−10.571	9.481	3.118	−10.515	10.108
Goods Island	3.117	−7.986	7.288	2.656	−5.288	7.131	4.075	−14.676	10.746
Turtle Head	9.069	−20.589	15.197	2.507	−7.945	7.410	6.446	−19.493	14.706
Ince Point	3.709	−7.296	9.868	2.286	−4.368	4.838	5.524	−12.278	12.104
Port Moresby	1.732	−5.132	4.424	1.802	−3.586	3.774	4.764	−9.914	11.116
Lae	9.065	−31.541	14.647	2.636	−5.059	6.417	12.772	−21.540	37.050
Lombrum Manus Island	5.384	−16.183	12.408	7.503	−21.352	19.381	7.801	−24.257	26.038
Madang	5.028	−10.084	10.805	3.302	−8.086	11.875	4.926	−12.724	8.713
Rabaul	16.816	−38.919	44.298	4.562	−13.195	16.909	9.395	−31.346	26.178

Table A.4b:

Tide gauge site	K1			O1			Q1		
	RMS	MIN	MAX	RMS	MIN	MAX	RMS	MIN	MAX
Exmouth	5.053	−10.095	9.610	2.354	−7.271	9.027	10.333	−35.197	29.083
Onslow Beadon Creek	6.871	−18.433	15.204	2.135	−6.125	5.053	10.576	−23.628	37.176
Port Hedland	6.156	−14.774	15.214	2.720	−8.343	7.518	11.818	−35.868	36.878
Broome	5.190	−12.325	15.176	3.152	−6.641	9.344	10.070	−23.765	24.946
Darwin	4.051	−8.099	10.497	3.786	−7.463	8.309	8.823	−22.294	20.260
Booby Island	2.859	−7.772	6.297	3.153	−7.803	8.308	10.064	−19.986	26.967
Goods Island	2.491	−6.120	5.664	3.193	−8.234	7.430	10.306	−24.607	25.770
Turtle Head	2.709	−7.499	6.031	4.712	−9.128	12.599	12.708	−29.705	35.061
Ince Point	2.354	−6.225	6.065	5.923	−10.601	12.264	13.247	−24.992	35.061
Port Moresby	1.627	−3.371	2.908	1.371	−2.827	3.431	10.026	−22.558	23.421
Lae	2.519	−3.135	6.303	3.715	−18.933	2.252	28.710	−26.510	146.00
Lombrum Manus Island	1.571	−4.729	4.734	3.285	−7.329	8.962	11.702	−29.459	32.506
Madang	1.419	−3.855	2.449	2.102	−5.452	6.489	10.328	−25.297	23.536
Rabaul	1.905	−5.070	7.950	2.499	−6.035	7.432	13.103	−34.071	32.276

Table A.4c:

Tide gauge site	K2			P1			2N2		
	RMS	MIN	MAX	RMS	MIN	MAX	RMS	MIN	MAX
Exmouth	1.761	−4.532	6.905	5.053	−10.095	9.610	3.329	−6.414	14.078
Onslow Beadon Creek	1.220	−2.259	3.004	6.871	−18.433	15.204	2.357	−6.334	7.329
Port Hedland	0.977	−2.150	2.319	6.156	−14.775	15.213	2.011	−3.779	4.867
Broome	0.833	−1.934	1.951	5.190	−12.325	15.176	1.818	−4.089	5.098
Darwin	0.807	−3.392	1.735	4.051	−8.099	10.497	1.519	−4.088	3.658
Booby Island	2.999	−10.570	9.482	2.859	−7.772	6.297	3.118	−10.515	10.108
Goods Island	2.656	−5.288	7.131	2.491	−6.120	5.664	4.075	−14.676	10.746
Turtle Head	2.507	−7.945	7.410	2.709	−7.499	6.031	6.446	−19.493	14.706
Ince Point	2.286	−4.367	4.839	2.354	−6.225	6.065	5.524	−12.277	12.105
Port Moresby	1.802	−3.585	3.775	1.627	−3.371	2.908	4.764	−9.915	11.115
Lae	2.636	−5.059	6.417	2.519	−3.135	6.303	12.772	−21.540	37.050
Lombrum Manus Is	7.503	−21.353	19.380	1.571	−4.729	4.734	7.801	−24.257	26.038
Madang	3.302	−8.086	11.875	1.419	−3.855	2.449	4.926	−12.724	8.713
Rabaul	4.562	−13.195	16.909	1.905	−5.070	7.950	9.395	−31.346	26.178

Data availability

The authors do not have permission to share data.

References

Australian Hydrographic Office, 2024. Hydroscheme industry partnership program (HIPP) statement of requirements (SOR). SPEC_03_33_BN38062220_HIPP_SOR_2025.1.pdf.

Bell, C., Vassie, J.M., Woodworth, P.L., 1996. The Tidal Analysis Software Kit (TASK Package). Dated 1 January 1996. TASK-2000 version dated December 1998. National Oceanography Centre: Liverpool. 20pp.

Birol, F., Fuller, N., Lyard, F., Cancet, M., Niño, F., Delebecque, C., et al., 2017. Coastal applications from nadir altimetry: example of the X-TRACK regional products. Adv. Space Res. 59 (4), 936–953. https://doi.org/10.1016/j.asr.2016.11.005.

Caldwell, P.C., Merrifield, M.A., Thompson, P.R., 2015. Sea Level Measured by Tide Gauges from Global Oceans — the Joint Archive for Sea Level Holdings (NCEI Accession 0019568), Version 5.5. NOAA National Centers for Environmental Information, Dataset. https://doi.org/10.7289/V5V40S7W.

Carrère, et al., 2022. A new barotropic tide model for global ocean: FES2022, OSTST 2022. https://doi.org/10.24400/527896/a03-2022.3287.

Cartwright, D.E., Tayler, R.J., 1971. New computations of the tide-generating potential. Geophys. J. Int. 23 (1), 45–73. https://doi.org/10.1111/j.1365-246X.1971.tb01803.x.

Codiga, D.L., 2011. Unified Tidal Analysis and Prediction Using the Utide Matlab Functions. Graduate School of Oceanography, University of Rhode Island, Narragansett, RI, p. 59. Technical Report 2011-01. ftp://www.po.gso.uri.edu/pub/downloads/codiga/pubs/2011Codiga-UTide-Report.pdf.

Egbert, G.D., Erofeeva, S.Y., 2002. Efficient inverse modelling of barotropic ocean tides. J. Atmos. Oceanic Technol. 19, 183–204. https://doi.org/10.1175/1520-0426(2002)019<0183:EIMOBO>2.0.CO;2.

Egbert, G.D., Erofeeva, S.Y., Ray, R.D., 2010. Assimilation of altimetry data for nonlinear shallow-water tides: Quarter-diurnal tides of the Northwest European shelf. Cont. Shelf Res. 30, 668–679. https://doi.org/10.1016/j.csr.2009.10.011.

Feng, X., Tsimplis, M.N., Woodworth, P.L., 2015. Nodal variations and long-term changes in the main tides on the coasts of China. J. Geophys. Res. Oceans 120. https://doi.org/10.1002/2014JC010312.

Filmer, M.S., Johnston, P.J., Jayaswal, Z., Taylor, A., Chittleborough, J., Claessens, S.J., Seifi, F., Kuhn, M., McCubbine, J., Entel, M., 2024. Connecting land and sea vertical datums: a data evaluation for developing Australia's AUSHYDROID model. Mar. Geod. 47 (3), 183–213. https://doi.org/10.1080/01490419.2024.2305898.

Foreman, M.G.G., 2004. Manual for tidal heights analysis and prediction. Pacific Marine Sci. Report 77-10, Inst. Ocean Sci. Patricia Bay, Victoria, B.C., 101 pages. (Online revised version of 1977 original).

Godin, G., 1972. The Analysis of Tides. University of Toronto Press, Toronto, Canada, p. 264.

Haigh, I.D., Marcos, M., Talke, S.A., Woodworth, P.L., Hunter, J.R., Hague, B.S., Arns, A., Bradshaw, E., Thompson, P., 2022. GESLA Version 3: a major update to the global higher-frequency sea-level dataset. Geosci. Data J. https://doi.org/10.1002/gdj3.174.

Hart-Davis, M.G., Piccioni, G., Dettmering, D., Schwatke, C., Passaro, M., Seitz, F., 2021. EOT20: a global ocean tide model from multi-mission satellite altimetry. Earth Syst. Sci. Data 13, 3869–3884. https://doi.org/10.5194/essd-13-3869-2021.

Hart-Davis, M.G., Andersen, O.B., Ray, R.D., Zaron, E.D., Schwatke, C., Arildsen, R.L., Dettmering, D., Nielsen, K., 2024. Tides in complex coastal regions: early case studies from wide-swath SWOT measurements. Geophys. Res. Lett. 51, e2024GL109983. https://doi.org/10.1029/2024GL109983.

Lyard, F.H., Allain, D.J., Cancet, M., Carrère, L., Picot, N., 2021. FES2014 global ocean tide atlas: design and performance. Ocean Sci. 17 (3), 615–649. https://doi.org/10.5194/os-17-615-2021.

Morrow, R., Fu, L.-L., Ardhuin, F., Benkiran, M., Chapron, B., Cosme, E., et al., 2019. Global observations of fine-scale ocean surface topography with the Surface Water and Ocean Topography (SWOT) mission. Front. Mar. Sci. 6, 232. https://doi.org/10.3389/fmars.2019.00232.

Parker, B.B., 2007. Tidal Analysis and Prediction. NOAA Special Publication NOS CO-OPS 3, US Department of Commerce. Silver Spring, Maryland, USA. https://tidesandcurrents.noaa.gov/publications/Tidal_Analysis_and_Predictions.pdf.

Pawlowicz, R., Beardsley, B., Lentz, S., 2002. Classical tidal harmonic analysis including error estimates in MATLAB using T_Tide. Comput. Geosci. 28, 929–937. https://doi.org/10.1016/S0098-3004(02)00013-4.

Pugh, D., Woodworth, P., 2014. Sea-Level Science: Understanding Tides, Surges, Tsunamis and Mean Sea-Level Changes. Cambridge University Press.

Ray, R.D., 2017. On tidal inference in the diurnal band. J. Atmos. Ocean. Technol. 34, 437–446. https://doi.org/10.1175/JTECH-D-16-0142.1.

Ray, R.D., Egbert, G.D., Erofeeva, S.Y., 2011. Tide predictions in shelf and coastal waters: status and prospects. In: Vignudelli, S., et al. (Eds.), Coastal Altimetry. Springer-Verlag, Berlin, pp. 191–216. https://doi.org/10.1007/978-3-642-12796-0_8 (Chapter 8.

Schureman, P., 1958. Manual of harmonic analysis and prediction of tides. Special Publication 98, Coast and Geodetic Survey, U.S. Dept. of Commerce, Washington, D. C., p. 317 (Revised 1940 Edition with corrections; first published in 1924).

Seifi, F., Filmer, M.S., 2023. Residual M_2 and S_2 ocean tide signals in complex coastal zones identified by X-Track reprocessed altimetry data. Cont. Shelf Res. 261, 105013. https://doi.org/10.1016/j.csr.2023.105013.

Wessel, P., Smith, W.H.F., Scharroo, R., Luis, J.F., Wobbe, F., 2013. Generic mapping tools: improved version released. EOS Trans. AGU 94 (45), 409–410. https://doi.org/10.1002/2013EO450001.

Woodworth, P.L., Vassie, J.M., 2022. Supplement of "Reanalyses of Maskelyne's tidal data at St. Helena in 1761". Supplement of Earth Syst. Sci. Data 14, 4387–4396. https://doi.org/10.5194/essd-14-4387-2022-supplement.

Woodworth, P.L., Pugh, D.T., Plater, A.J., 2015. Sea-level measurements from tide gauges. In: Shennan, Ian, Long, Antony J., Horton, Benjamin P. (Eds.), Handbook of Sea-Level Research, first ed. John Wiley & Sons, Ltd, pp. 557–574. Chapter 35.

Woodworth, P.L., Hunter, J.R., Marcos, M., Caldwell, P., Menéndez, M., Haigh, I., 2017. Towards a global higher-frequency sea level dataset. Geosci. Data J. 3, 50–59. https://doi.org/10.1002/gdj3.42.

Lyard, F.H., Carrère, L., Fouchet, E., Cancet, M., Greenberg, D., Dibarboure, G., Picot, N. (in preparation) FES2022: a Step Towards a SWOT-compliant Tidal Correction, to be Submitted to Ocean Sciences.